Accepted Manuscript

Identifying temporally and spatially changing boundary conditions at an aquifer – Aquitard interface using helium in porewater

D. Rufer, H.N. Waber, T. Gimmi

PII: S0883-2927(18)30144-6

DOI: 10.1016/j.apgeochem.2018.05.022

Reference: AG 4099

To appear in: *Applied Geochemistry*

Received Date: 29 December 2017

Revised Date: 24 May 2018

Accepted Date: 31 May 2018

Please cite this article as: Rufer, D., Waber, H.N., Gimmi, T., Identifying temporally and spatially changing boundary conditions at an aquifer – Aquitard interface using helium in porewater, *Applied Geochemistry* (2018), doi: 10.1016/j.apgeochem.2018.05.022.

Identifying temporally and spatially changing boundary conditions at an aquifer – aquitard interface using helium in porewater

D. Rufer [a,*], H.N. Waber [a] and T. Gimmi [a, b]

[a] RWI, Institute of Geological Sciences, University of Bern, CH-3012 Bern, Switzerland
[b] Paul Scherrer Institut, CH-5232 Villigen, Switzerland

* Corresponding author: Daniel Rufer, Institute of Geological Sciences, Baltzerstrasse 1+3, CH-3012 Bern, Switzerland; email: daniel.rufer@geo.unibe.ch

Abstract

Helium concentrations and $^{3}He/^{4}He$ isotope ratios of porewater, groundwater and rock were measured on samples collected from a Jurassic sediment sequence at the Mont Terri underground rock laboratory (Northern Switzerland). Porewater He data of rock samples collected from borehole BDB-1 at high spatial resolution across a karstic limestone unit (Passwang Formation) into the underlying claystone sequence (Opalinus Clay, Staffelegg Formation) describe a continuous profile from the water-conducting zone in the limestone into the clay-rich rocks of low permeability. Concentrations of ^{4}He, ^{3}He and their parent nuclides in the rock allow calculating in-situ production and accumulation terms. Since the time of sedimentation, 90% - 97% of the in-situ produced ^{4}He has been released to the porewater. Today only 2.5% of the maximum possible accumulated ^{4}He is still retained in the porewater while the major part of in-situ produced ^{4}He was removed from the system presumably by porewater–groundwater exchange. The porewater ^{4}He concentrations show a diffusion profile from the aquitard towards the aquifer, reflecting a) a transient state

between ^{4}He in-situ production and porewater–groundwater exchange, b) a transient state from previously higher ^{4}He concentrations in the porewater, and c) a spatially variable boundary in the karstic limestone unit. Evolutionary models of porewater ^{4}He concentration profiles in combination with constraints from independent chemical and isotopic tracers allow deciphering a complex palaeo-hydrogeological history of the system over about the last 30 ka. A local excursion from the general profile towards higher ^{4}He concentrations and ^{3}He/^{4}He ratio in a limestone layer in the Opalinus Clay cannot be further constrained in time based on the present sample frequency, but appears to represent a hydrogeological signal.

Keywords: Helium, dissolved noble gas, porewater chemistry, groundwater, diffusion, modelling

1. Introduction

Clay-rich sedimentary rock sequences are characterised by low hydraulic conductivity and solute transport dominated by diffusion (Falck et al., 1990; Gimmi and Waber, 2004; Gimmi et al., 2007; Mazurek et al., 2009, 2011; Pearson et al., 2003; Rübel et al., 2002; Savoye et al., 2008). As such, they are natural archives of groundwater evolution in their bounding aquifers. The variable shapes of concentration profiles developed for different tracers from the bounding aquifer into the aquitard allows constraining transport conditions in such systems over a wide range of spatial and temporal scales (e.g. Gimmi and Waber, 2004; Gimmi et al., 2007; Mazurek et al, 2009, 2011). Acting as natural barriers in hydraulic systems, clay sequences of low permeability are investigated for their potential as host rocks for radioactive waste repositories and as caprocks for hydrocarbon reservoirs or CO_2 sequestration.

In Switzerland, the Opalinus Clay is investigated as a potential host rock for radioactive waste (Nagra 2002). As an analogue, this clay formation has also been investigated at the Mont Terri underground rock laboratory (URL) in the Jura mountains of northern Switzerland since 1996 (e.g. Bossart et al., 2017). In 2013/14 a deep borehole (Borehole BDB-1) was core drilled for the first time across the entire Opalinus Clay including its hanging wall and footwall whereas previous studies had to rely on short boreholes drilled at various locations along the URL. Borehole BDB-1 aimed at long-term hydraulic monitoring (Jaeggi et al., 2016; Yu et al., 2017), porewater geochemistry and aquifer-aquitard interface studies (Waber and Rufer, 2017; Yu, 2017), method comparison of porewater extraction techniques (Mazurek et al., 2017) as well as detailed stratigraphic studies (Hostettler et al., 2017). The design of the drilling and core sampling allowed, for the first time, collecting samples for porewater chemical, isotope and noble gas tracers on the dm- to m scale along a borehole profile across the entire sedimentary sequence.

Helium is a powerful tracer to investigate hydrogeological systems due to its chemical inertness, low abundance in air and air-saturated water, and high diffusivity in porewater. Its distinctive property of geogenic in-situ production makes it an ideal complement to conservative chemical and isotope tracers for temporally constraining hydrogeological processes. Porewater He concentrations in clay-rich sequences have been investigated in different hydrogeological settings such as the Triassic sedimentary sequence in Morsleben, Germany (Osenbrück et al., 1998), the Opalinus Clay in the Swiss Molasse Basin (Mazurek et al., 2009; Nagra, 2001; Rufer and Waber, 2015) and in the folded Jura Mountains at Mont Terri (Mazurek et al. 2009, 2011; Rübel et al., 2002), the Callovo-Oxfordian shale in the Paris Basin (Battani et al., 2011; Bigler et al., 2005; Jean-Baptiste et al., 2016; Waber, 2012), the fractured Tournemire shale in Southern France (Bensenouci et al., 2011), the Boom Clay in

Belgium (Mazurek et al., 2009, 2011), and the Ordovician shale in the Michigan Basin, Canada (Clark et al., 2013). These previous studies focussed mainly on the characterisation of solute transport over large spatial and temporal scales, with sample spacings on the scales of decametres or more. Consequentially, model fits are characterised by large degrees of freedom due to the rather isolated, punctual data base and the resolution in time for the evolution of observed concentration profiles is limited. In addition, most of these model scenarios are based on the implicit premise of mostly invariant boundary conditions and stable geological settings over the (long) model durations in the order of millions of years.

The present study explores the porewater – groundwater exchange between the Opalinus Clay and the overlying karstic limestone sequence on time scales of <1 Ma. This was attempted by producing He concentration profiles (^{4}He, ^{3}He/^{4}He) in porewater at high spatial resolution. Special emphasis was given to possible effects of spatially moving boundary conditions during the past palaeo-hydrogeological evolution. The interpretation and quantitative description of obtained He tracer profiles take advantage of other chemical (Cl, Br) and isotope (δ^{18}O, δ^2H, δ^{37}Cl) tracer profiles produced at the same spatial resolution and described in Waber and Rufer (2017).

2. Geological setting

The Mont Terri URL is located in the southern limb of the Mont Terri anticline, which consists of Triassic evaporites, marls and dolomite in the core, clay-rich sequences of Lower Jurassic age in the centre and Malm limestones at the top (Bossart et al., 2017; Nussbaum et al., 2011). In this anticline, the Opalinus Clay (OPA), an over-consolidated claystone of Aalenian / Toarcian age, is intercalated between the 229 m thick sequence of variable

oolithic carbonates, limestones and marlstones of the Hauptrogenstein (HRST) and Passwang Formation (PAF) of Bajocian age on top and the marlstones and bituminous claystones of the Staffelegg Formation (STF) of Toarcian age at the bottom (Fig. 1; Hostettler et al., 2017; Reisdorf et al., 2014). The sedimentary sequence experienced its maximum burial of about 1350 m with a maximum temperature of 85°C during the Cretaceous (Mazurek et al., 2006) and was exhumed and partially eroded during the late Cretaceous and Paleogene. The Jura folding between about 12-3 Ma led to the development of the Mont Terri anticline at the junction of the frontal part of the Jura fold-belt and the Rhine-Bresse transfer zone (Nussbaum et al., 2011, 2017). Subsequently, erosive exposure of the top of the Middle Jurassic limestones overlying the Opalinus Clay occurred some 2.5 Ma ago and that of the underlying Early Jurassic strata about 350 ka ago (Bossart and Wermeille, 2003). Since then, freshwater infiltration into these bounding formations has been possible, as evidenced by karstic water-conducting features in the Passwang Formation and the Late Triassic Gryphaea limestones.

Along borehole BDB-1, the Opalinus Clay has a thickness of 130 m and the strata dips towards SSE with dip angles ranging from 65° in the Hauptrogenstein to 45° in the Opalinus Clay (Hostettler et al., 2017). A major thrust fault zone, the so-called "Main Fault", is encountered in the borehole at 226 – 227 m BHL (Jaeggi et al., 2017; Nussbaum et al., 2017).

Drilled in 2013/14, the inclined, 247.5 m long borehole BDB-1 has a mean azimuth and dip of 330°/44°, which is roughly perpendicular to the local bedding. The borehole cuts across the lower Hauptrogenstein-Formation (0 – 37.07 m BHL), the Passwang-Formation (37.07 – 106.15 m BHL) and the Opalinus Clay (106.15 – 238.08 m BHL) into the Staffelegg-

Formation. At 58.6 m BHL in the limestones of the Passwang-Formation, a water inflow was detected and sampled using a single packer system. Across the Hauptrogenstein and Passwang Formation, the borehole was water-drilled with low-mineralised, recent groundwater from the Hauptrogenstein as drilling fluid. Across the Opalinus Clay and into the Staffelegg Formation, the borehole was air-drilled. The entirety of the borehole was cored using a wireline coring system, with core diameters of 101 mm for the first section and 85 mm for the second section. Further technical details of the drilling are given in Jaeggi et al. (2016).

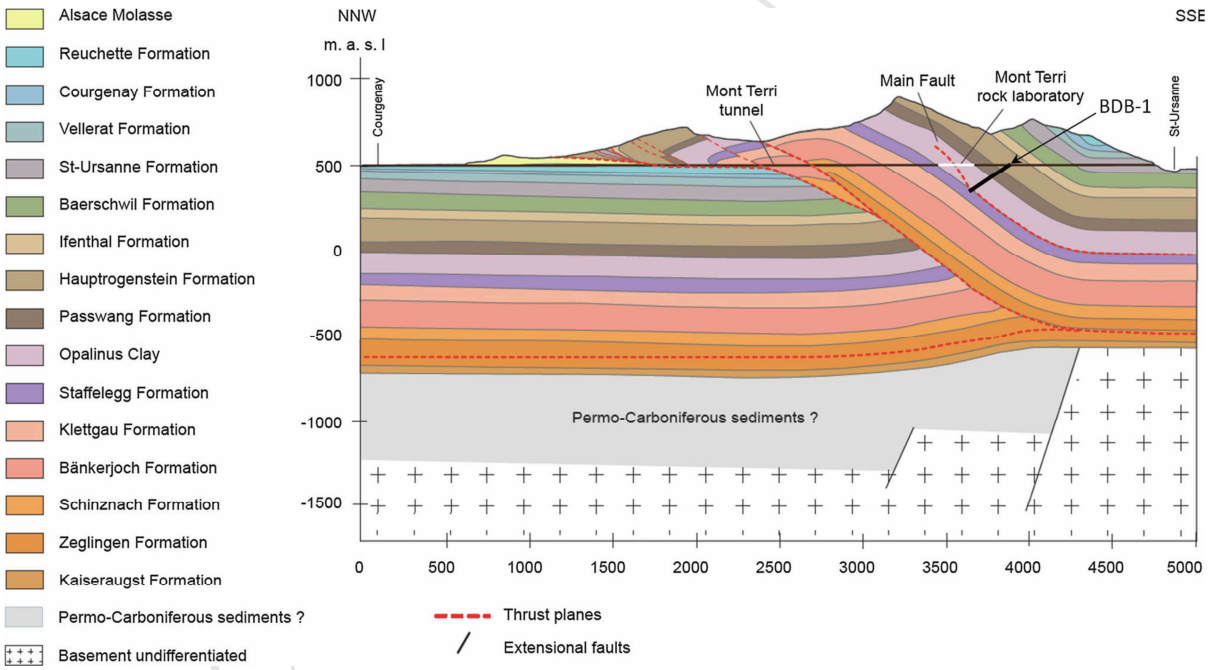

Fig. 1. Geological cross-section of the Mont Terri anticline with the location of the Mont Terri underground rock laboratory (white line). The deep borehole BDB-1 (thick black line) crosses the lower part of a karstic aquifer located in the Hauptrogenstein Formation, the entire Opalinus Clay formation and the upper part of the Liassic marls (adapted from Nussbaum et al. 2017)

The rock sequences encountered by borehole BDB-1 consist of limestones to claystones of variable spatial extent and composition. A detailed lithostratigraphic description is given in Hostettler et al. (2017). Petrographical and mineralogical data of all BDB-1 drillcore samples is given in Waber and Rufer (2017) and Yu (2017) and clay contents deduced from gamma ray logs in Willenberg-Spillmann (2015). The Hauptrogenstein section encountered in the borehole consists primarily of limestones with gamma ray logs indicating low clay contents. The Passwang Formation constitutes a highly variable alternation of limestones, marls and sandstones with variable clay, carbonate and sand contents. Clay contents range from 9 to 39 wt.%, in agreement with the data from geophysical logs. The Opalinus Clay displays a more homogeneous composition of claystones to silty claystones (shaly facies 1 and 2) and claystones with intercalated limestone and sandstone layers (sandy facies 1 and 2). Clay contents show a general increase with depth, with average values of 44 wt.% in sandy facies 2 and 59 wt.% in shaly facies 1. Markedly lower values down to 8 wt.% are measured in sandy facies 1 and the carbonate-rich sandy facies. These lower clay contents are corroborated by the gamma ray logs and are spatially limited. The uppermost Staffelegg Formation below the contact to the Opalinus Clay consists of argillaceous limestones and clayey to bituminous marls with clay contents decreasing down to 36 wt.% near the borehole's terminal depth at 247.5 m BHL.

Several open fractures were identified throughout the Hauptrogenstein and the topmost Passwang Formation down to 40 m BHL and again from 48-50 m BHL by macroscopic core mapping and geophysical and borehole imaging logs (Fischer, 2014; Jäggi et al., 2016). Based on pronounced increases in temperature and electric conductivity in the borehole logs, flowing groundwater is suspected at several locations across the lower Hauptrogenstein and the upper Passwang Formation (Fischer, 2014). While no borehole logs are available from

50 – 97 M BHL, a water inflow of 5-10 L/min was detected in this interval and is associated to open fractures observed in the drillcore between 58.5 and 58.8 m BHL (Jaeggi et al., 2016).

Further accumulations of open fractures, but without indications of flowing groundwater, were observed from 62-65 m BHL, 72-74 m BHL, at 77.6 m BHL and between 98-100 m BHL in the Passwang Formation. In the Opalinus Clay a few wet spots around weak tectonic structures were observed without noticeable water flow.

3. Methodology

3.1 Drillcore sampling

Aiming at a continuous geochemical record between the encountered aquifer in the Passwang Formation and the Opalinus Clay, core samples were taken with increased sampling frequency closer to the aquifer. At completion of borehole BDB-1, 25 samples for dissolved noble gas analyses were collected together with over 200 samples for porewater investigations and other purposes in the context of the "Opalinus Clay – Passwang Interface" programme. A detailed description of the sampling and analytical procedures and the complete sample inventory of borehole BDB-1 is given in Waber and Rufer (2017).

A stringent sampling protocol was followed to preserve the in-situ water saturated state of the rock material during sampling and to minimise potential sample contamination with extrinsic fluids or gases (drilling fluid, air) and all relevant data (e.g. exposure duration to air) was recorded to later allow forensic identification of potential causes for observed artefacts (Waber and Rufer 2017). After recovery, the core sections were immediately sealed into transparent plastic tubes and evacuated to inhibit desiccation and gas exchange with the air

and to allow a first geologic survey. For noble gas measurements in porewater, core samples were collected using existing bedding-parallel breaks caused by disking if possible, otherwise they were trimmed by dry-cutting on a rock saw. Sections of roughly 15 cm length of the central parts of lithologically homogeneous core were trimmed to ca. 150 cm^3 cuboids by dry sawing to remove the partly degassed and contaminated rim of the core. The large sample size was chosen to optimise the ratio of potentially contaminated to uncontaminated porewater volume. After recording its wet weight, the cuboid was immediately placed in a stainless-steel container with a ConFlat (CF) sealed lid fitted with a copper tube. After sealing, the entrapped air was removed by gently pumping the container to roughly 5-10% of the initial gas pressure followed by flushing with N_2 (99.99% purity). This was repeated three times, allowing to efficiently pump off residual air without inducing sample degassing. After a last pumping step, the container was vacuum-sealed by crimping the copper tube with two screw-driven steel clamps during final pumping and then stored at ambient temperature. Exposure times to air of the central cuboids are narrowly confined, with an average of less than 6 minutes.

3.2 Groundwater sampling

After detection of the water inflow, an interval from 51 - 59.65 m BHL was packed off by single packer (Jaeggi et al., 2016). Interval pressure stabilised at 7 bars and the measured outflow rate was 2 L/min. The latter was, however, limited by the diameter of the sampling line, as the observed flow rate prior to the packer installation was 5-10 L/min. After a flushing time of 18 hours (over 10 times the interval volume), three sets of groundwater samples were collected for chemical, stable and radiogenic isotope and noble gas analyses over the course of 36 hours (Waber and Rufer, 2017). For noble gas analysis, groundwater

was collected in-line into copper tubes to avoid contact between groundwater and air. The tubes were filled from bottom to top and simultaneously tapped with a metal bar to ensure complete removal of all air bubbles from the sample and then clamped off by steel clamps.

3.3 Helium and neon analysis of porewater and groundwater

Determining porewater concentrations of dissolved noble gases is based on their quantitative release from the porewater (e.g. Osenbrück et al., 1998; Rübel et al., 2002) due to their low solubility in water under ambient conditions (Weiss, 1971). Their chemical inertness inhibits any reaction during out-gassing, allowing calculation of their porewater concentration from the released amount of gas and the mass of porewater of the rock sample.

The dissolved porewater gases were quantitatively released from the porewater by molecular diffusion into the container's void volume over the course of 2 to 16 months at a constant temperature of 20.5 ± 0.5°C. After this time, less than 1% of He stays dissolved in the porewater of sedimentary rocks (Bigler et al., 2005; Osenbrück et al., 1998). The released gas was extracted from the sample container by expansion into a large volume, which was then rapidly closed off to minimise artefacts due to pressure-change induced disturbances of the equilibrated gas composition. Helium and Ne were then separated and purified from the extracted gas by a sequential combination of water traps, chemical getters operated at 650°C (Ti-sponge) and ambient temperature (SAES GP50), and a liquid-N_2 cooled cold trap filled with activated charcoal.

Amounts of ^{4}He and Ne and ^{20}Ne/^{22}Ne ratios were determined at the Institute of Geological Sciences, University of Bern, Switzerland, using a Pfeiffer QMS200 quadrupole mass spectrometer equipped with an in-line faraday cup detector, operated in static mode (Poole

et al., 1997). All samples were analysed in duplicate. The analyses were referenced against air (5.24 ppmv He; 18.18 ppmv Ne; $^{20}Ne/^{22}Ne$ = 9.78; de Laeter et al., 2003) and against air that was enriched with 99.99 % pure He (isobaric, volumetric mixture) to 1073 ± 81 ppmv He. All analyses of the calibration gases reproduce the reference values within 1σ RSD (relative standard deviation) of 2% (He), 3% (Ne) and 7% ($^{20}Ne/^{22}Ne$). A purified aliquot of He was later analysed for $^{3}He/^{4}He$ ratios at the Institute of Environmental Physics, University of Bremen, Germany, according to the procedure given in Sültenfuss et al. (2009).

Measured Ne concentrations were used to assess air contamination of the sample gas (e.g. Bigler et al., 2005; Rübel et al., 2002; Waber, 2012) as Ne has a negligible in-situ geogenic production (Leya and Wieler, 1999), with $^{20}Ne/^{22}Ne$ ratios < 1; (Ballentine and Burnard, 2002). Any measured Ne with atmospheric $^{20}Ne/^{22}Ne$ ratio and concentration exceeding that of air-saturated water (Ne_{asw} approximately 1.9×10^{-7} ccSTP/g_{H2O}; Weiss, 1971) is therefore attributed to air contamination. Using the relative atmospheric abundance of Ne and He, the concentration of contaminant air and air-derived excess helium ($air_{contaminant}$; He_{excess}, both given as ccSTP/g_{pw}) in the sample porewater can be calculated as

$$air_{contaminant} = \frac{Ne_{meas} - Ne_{asw}}{Ne_{air}} \quad (1)$$

$$He_{excess} = air_{contaminant} * He_{air} \quad (2)$$

where Ne_{meas} is the Ne concentration in the gas sample in ccSTP/g_{pw}, Ne_{asw} is the Ne concentration in air-saturated water, and Ne_{air} and He_{air} are the relative volumetric abundances of Ne and He in air (18.18 and 5.24 ppmv, respectively; de Laeter et al., 2003).

To obtain the ^{4}He concentration in porewater, $^4He_{pw}$ (in ccSTP/g_{pw}), the measured amount of ^{4}He, $^4He_{meas}$, in the sample gas is corrected for air-derived He, He_{excess}, and divided by the mass of the porewater, m_{pw}, (see 3.5).

Measured Ne concentrations in the BDB-1 porewater are low ($Ne_{pw} < 1.9\times10^{-6}$ ccSTP/g_{pw}, Table 3), translating into relative air contaminations of the gas in the sample containers of <11.2 vol.% ("BDB-1 maximum relative air contamination" in Fig. 2). As ^{4}He concentrations in porewater of the Opalinus Clay are generally high and the partial pressure of He in the gas of the porewater samples usually exceeds the atmospheric partial pressure of He by at least one to two orders of magnitude, air-derived He_{excess} constitutes less than 1% of $^4He_{meas}$ in the BDB-1 samples. While being corrected for, this does not affect measured $^4He_{meas}$ concentrations or ^{3}He/^{4}He ratios beyond analytical uncertainties (Fig. 2). However, due to its high concentration in sample porewaters, He is prone to degassing and any prolonged contact of the sample with air during sampling leads to He loss from the sample porewater, emphasizing the need for efficient and disciplined sampling.

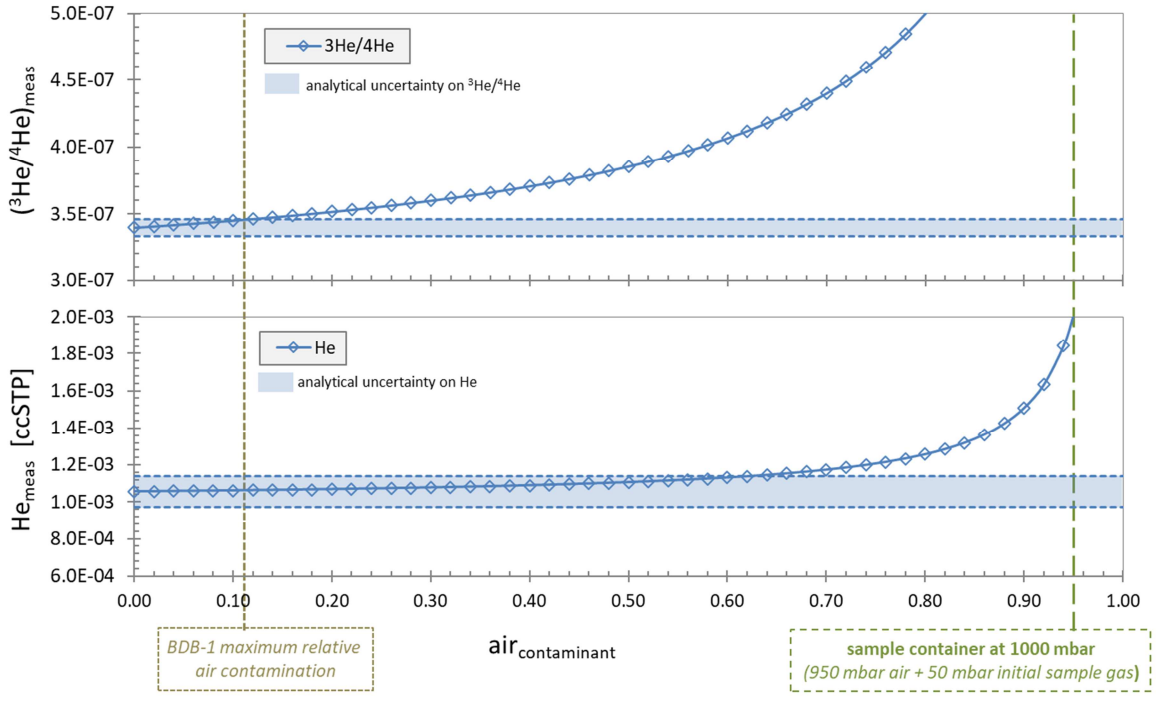

Fig. 2. Example of the effect of increasing air contamination on the measured amount and isotope ratio of He ($^4He_{meas}$, $(^3He/^4He)_{meas}$) from an uncontaminated core sample. The pressure of the uncontaminated sample gas in the container is assumed to be 50 mbar, of which 5.5×10^{-3} mbar is He. This sample gas was outgassed from 17.6 g porewater with a He concentration of 6.0×10^{-5} ccSTP/g_{pw} and a $^3He/^4He$ ratio of 3.4×10^{-7}, which is representative for an average sample of Opalinus Clay from borehole BDB-1.

It is not a priori possible to attribute lower porewater He concentrations to either a hydrogeological signal or to a sampling artefact. Observation of an elevated air contamination can therefore be used to distinguish between the two.

Noble gas concentrations in the groundwater samples were analysed at EAWAG, Dübendorf, Switzerland, according to the procedure given in Beyerle et al. (2000).

3.4 Helium and parent radionuclide analyses of bulk rock

Bulk rock concentrations of U, Th, K, Li and ^4He were measured on representative aliquots of 8 noble gas core samples at the Kola Scientific Centre in Apatity and by Neva Geological Expedition in St. Petersburg, Russia. Element concentrations were measured by X-ray fluorescence spectrometry (U and Th) and by atomic absorption spectrometry on completely digested rock material (K and Li). The abundance of ^4He was determined by fusion of dried bulk rock at 1600°C, followed by purification and separation of the released gas with Ti-Zr getter and liquid-N_2 cooled cold traps, and subsequent measurement by mass spectrometry as described in Tolstikhin et al. (2011). Any ^4He originally dissolved in the porewater was removed by out-gassing prior to bulk rock analysis. The analytical uncertainties (1σ RSD) for these measurements as reported by the laboratories are ± 10% for U and Th, ± 3%, for K and ± 20% for Li, with ^4He blanks being below 1×10^{-6} ccSTP/g_{rock}.

3.5 Petrophysical measurements

The mass of porewater, m_{pw}, was determined gravimetrically as the difference between the wet weight of the cuboid at the time of sampling on site and after gas-equilibration by drying to constant weight in a ventilated oven at 105°C up to 40 days. As the porewater in the Opalinus Clay at Mont Terri has an ionic strength well below that of seawater (Pearson et al., 2003), no salinity correction has been applied and the density of the porewater (ρ_{pw}) is taken as 1.00 g/cm^3. The water content of the rock sample relative to its wet weight (WC_{wet}) is then calculated as the porewater mass relative to the sample's wet weight.

Grain density (ρ_g) was measured by the He-gas displacement technique on a Micrometric AccuPyc II 1340 gas-pycnometer. About 7 g of dried powder (< 2µm) rock material equivalent to that of the noble gas sample lithology were analysed from core pieces adjacent to the noble gas core samples. The reported grain density is the average of 5 measuring cycles, of which the standard deviation (1 SD) has to be ≤ 0.005 g/cm^3.

The wet water-loss porosity or volumetric moisture content of a rock sample, $\phi_{WL\ wet}$, is calculated as the ratio of its water-filled, connected pore volume to its total volume according to:

$$\phi_{WL\,wet} = \frac{WC_{wet} * \rho_g}{WC_{wet} * \rho_g + (1 - WC_{wet}) * \rho_{pw}} \quad (3)$$

Unless noted otherwise, analytical uncertainties are given as 1σ (R)SD and were estimated using first order error propagation.

3.6 Modelling Procedures

In order to assess the potential evolution of the presently observed helium porewater concentration profile, a model was formulated with the geochemical transport code Flotran (Lichtner, 2007). This code can simulate heterogeneous flow and transport coupled with

kinetic or equilibrium geochemical reactions in up to three spatial dimensions. It solves the transport equations based on an integrated finite-volume difference method. Our model considers in-situ production of helium and one-dimensional diffusive transport of dissolved ^{4}He in the porewater perpendicular to bedding towards one or multiple boundaries. Two model setups were considered: one focusing on steady-state between a stable upper and lower boundary, and one focusing on transient diffusion towards a spatially and temporally variable upper boundary.

3.6.1 Model setup and parameters

For both model setups, the encountered lithologies along the BDB-1 borehole were divided into 4 zones with different properties (see below, Table 1) with an increasingly finer spatial discretisation towards the upper boundary located at the groundwater conducting fracture at 58.6 m BHL in the Passwang Formation. Model input parameters (Table 1) for petrophysical properties ($\phi_{WL,wet}$, ρ_g), in-situ accumulation rates of helium in porewater ($^4He_{acc}$) and diffusion coefficients (effective diffusion coefficient D_{eff}, pore diffusion coefficient $D_p = D_{eff}/\phi_{WL\ wet}$) in each model zone were calculated as averages of the available values of the formation's member units (or facies in the case of the Opalinus Clay) weighted by their thickness measured in borehole BDB-1. For the Opalinus Clay, a complete dataset of petrophysical properties and in-situ helium accumulation rates for the different facies was acquired in this study (Table 2, Table 4). For the Passwang Formation, average values were calculated based on available samples and for the Staffelegg Formation only the uppermost part was considered in the model and the available data from the Rietheim Member were used.

For the steady-state simulation, a two-sided diffusion domain was used with the upper boundary located at the groundwater conducting fracture in the Passwang Formation and an assumed lower boundary located at a virtual distance of 340 m BHL in the Gryphaea Limestone. This lower boundary position corresponds to the locality of this limestone unit in borehole BDB-1 when projected from the URL level where it was water-conducting (Gautschi et al., 1993). This results in a half-size of the domain of 140.7 m.

For the simulations focussing on transient diffusion towards a variable upper boundary, the modelled domain has a 1D geometry of 191.4 m length (from 58.6 m BHL to 250 m BHL), spanning the entire profile across borehole BDB-1 below the groundwater conducting fracture in the Passwang Formation. Zero solute flux was assumed as boundary condition on the lower side of the domain based on the observed $^4He_{pw}$ concentration profile and the absence of a water-conducting zone down to the bottom of borehole BDB-1. Time-dependent conditions were considered at the upper boundary of the domain, including intervals of zero solute flux and constant He concentrations (air saturated water) in the groundwater. In some scenarios, time-dependent concentrations were also considered for an internal node to simulate time-dependent activation or closing of high permeability zones at 73 m BHL ("proximal boundary" in Table 1) within the Passwang Formation. To handle such time-dependent external or internal conditions, the code Flotran was slightly adapted (see Waber et al., 2012). While model results fitting the measured $^4He_{pw}$ concentration in the Opalinus Clay are obtainable by a wide range of combinations of initial $^4He_{pw}$ concentrations and model evolution times, scoping model calculations showed that the curvature of the measured $^4He_{pw}$ profile in the Passwang Formation and uppermost Opalinus Clay can only be reasonably obtained for model evolution times <100 ka (see Fig. 6). Over such a period the accumulated in-situ produced helium merely amounts to

$<1.3\times10^{-6}$ ccSTP/g_{pw}, which has little influence on the $^4He_{pw}$ concentration in the lower part of the Opalinus Clay over the model time period. Therefore, initial $^4He_{pw}$ concentrations were set to a constant value of 5.7×10^{-5} ccSTP/g_{pw} over the entire profile, that is, about to the average value observed at present in the lower part of the profile.

This contrasts the assumption of a much higher initial $^4He_{pw}$ concentration in the porewater of 4.7×10^{-4} ccSTP/g_{pw} in the model of Mazurek et al. (2009, 2011), who, however, assume a constant and permanently flushed upper boundary over 6 Ma (based on Cl^- profile fitting). On one hand, assuming a stable hydrogeological setting at Mont Terri over such a long timescale may be debatable considering still ongoing tectonic activities and erosion processes; on the other hand, such a long-term model is unable to resolve shorter-term changes in the hydrogeological setting, which lead to lower order variations in the porewater He profile. This is e.g. indicated by a low accordance between the continuously curved model solution and the flatter measured porewater He profile in the Opalinus Clay in Mazurek et al. (2009, 2011).

Zone	**Lower boundary of zone**[1]	**$\phi_{WL\ wet}$**	**$D_{p\perp}$ (He)**	**$D_{eff\perp}$ (He)**	**$^4He_{acc}$**
	m BHL	vol.%	m^2/s	m^2/s	ccSTP/(g_{pw}*a)
PAF 1	76	9.92%	1.90E-9	1.88E-10	1.11E-11
PAF 2	106	9.92%	9.49E-10	9.41E-11	1.11E-11
OPA	238	13.13%	4.20E-10	5.53E-11	1.28E-11
STF	250	13.45%	3.99E-10	5.36E-11	1.10E-11

[1] Upper boundary of model domain at 58.6 m BHL

Boundary	**depth**	**$^4He_{gw}$**
	m BHL	ccSTP/g_{gw}
Present-day groundwater	58.6	4.6E-8 (air-saturated water)
Proximal boundary	73	4.6E-8 (air-saturated water)

Table 1: Model input parameters.

3.6.2 Helium Diffusion Coefficients

So far, only two diffusion coefficients for ^{4}He in Opalinus Clay at Mont Terri are reported in the literature: an experimental value ($D_{eff\,||\,(He)}$ = 2.1×10^{-10} m^2/s) by Gómez-Hernández (2000) and a best-fit model value ($D_{p\,(He)}$ = 3.5×10^{-11} m^2/s) based on a natural He concentration profile along the Mont Terri Tunnel (oblique to bedding) by Rübel et al. (2002). These values differ by over an order of magnitude and their validity is questioned due to issues related to drilling-related increased porosity (Gómez-Hernández, 2000; Jacops et al., 2013) in the first case, and due to the unsubstantiated assumption of a steady-state (diffusive loss of ^{4}He from the formation being balanced by in-situ production) in the second case (Jacops et al., 2013; Mazurek et al., 2009; Waber and Rufer, 2017). The only other diffusion coefficient for ^{4}He in Opalinus Clay was determined on a sample from 860 m depth from a deep borehole in the Molasse-Basin in NE Switzerland (Schlattingen) by Jacops et al. (2016). For this sample, these authors obtained perpendicular to bedding a pore diffusion coefficient $D_{p\,\perp\,(He)}$ of 7.13×10^{-10} m^2/s at a porosity of 9.6 vol.% what corresponds to an effective ^{4}He diffusion coefficient perpendicular to bedding $D_{eff\,\perp\,(He)}$ of 6.84×10^{-11} m^2/s.

For Mont Terri there is, however, a number of diffusion coefficients reported for HTO in Opalinus Clay, both experimentally determined and modelled from in-situ tracer profiles (e.g. Palut et al., 2003; Tevissen and Soler, 2003; Tevissen et al., 2004; Van Loon et al., 2004a,b; Van Loon et al., 2005; Wersin et al., 2004; Wersin et al., 2008; Yu, 2017). These $D_{eff\,\perp\,(HTO)}$ values range from 1.0×10^{-11} to 2.1×10^{-11} m^2/s for the shaly facies and from 1.8×10^{-11} to 2.1×10^{-11} m^2/s for the sandy facies (with $D_{eff\,||}$ values parallel to bedding being recalculated using an anisotropy coefficient ($D_{eff\,||}$ / $D_{eff\,\perp}$) of 4 (Van Loon et al., 2004a; Wersin et al., 2004). Using the ratio of the diffusion coefficients of He and HTO in free water

($D_{0(He)}/D_{0(HTO)}$) = 3.17; Cook and Herczeg, 2000), average $D_{eff\perp(He)}$ values of 4.85×10^{-11} m^2/s and 6.22×10^{-11} m^2/s are calculated for the shaly and sandy facies of the Opalinus Clay at Mont Terri, respectively, which is roughly comparable to the experimental value from Schlattingen by Jacops et al. (2016) given above. The formation level $D_{eff\perp(He)}$ values for Opalinus Clay were then calculated similar to the in-situ production terms as weighted average of the shaly and sandy facies values. For ^{4}He, the diffusion accessible porosity is taken as equal to the water loss porosity, $\phi_{WL\ wet}$, and pore diffusion coefficients for helium $D_{p\perp(He)}$ were accordingly calculated as

$$D_{p\perp}(He) = \frac{D_{eff\perp}(He)}{\phi_{WL\,wet}} \quad (4)$$

For the Staffelegg Formation, the He diffusion coefficients are based on the experimental $D_{eff\perp}$(HTO) value of 1.69×10^{-11} m^2/s from Yu (2017). For the Passwang Formation, no diffusion coefficients are available for uncharged tracers perpendicular to bedding. Available $D_{eff\perp(HTO)}$ values from the corresponding stratigraphic units in NE Switzerland ('Brauner Dogger' and Effingen Member in the boreholes Benken, Schlattingen, Oftringen and Gösgen) are, however, up to >3 times larger than the corresponding $D_{eff\perp(HTO)}$ of Opalinus Clay from the same sites (Van Loon, 2014). In spite of certain lithological differences, these samples are roughly comparable to the rocks from the Mont Terri Passwang Formation taking into consideration the strong lithological heterogeneity in these units. Based on this, the $D_{eff\perp}$ value for HTO (and, accordingly, the diffusion coefficients for He) for modelling the Passwang Formation at Mont Terri is kept loosely constrained to between 1 to 5 times that of the Opalinus Clay.

Hostettler et al. (2017) divide the Passwang Formation below 57 m BHL into three lithological zones, of which the upper two (57.1 – 76.4 m BHL) are predominantly composed

of alternations of sandy limestones and marls with intercalated quartz-sand-rich laminae below 61 m BHL, whereas the lowermost section (76.4 to top Opalinus Clay) is described as heterogeneously alternating marls and sandstone lenses and interspersed limonitic and sandy limestone beds. The contact between the upper two and the lowermost zone roughly coincides with the lower end of a low gradient plateau in the porewater ^{4}He concentration data (see 4.2), for which the break in slope indicates a possible difference in diffusion properties. The model domain for the Passwang Formation was therefore divided similarly into an upper (PAF 1) and lower (PAF 2) domain at 76 m BHL, with independent diffusion coefficients (Table 1).

4. Results

4.1 Petrophysical data

The gravimetrically determined mass of porewater present in the connected pore space of the originally saturated rock sample corresponds to the porewater where solute transport takes place in low-permeability rocks. Porewater masses, $m_{pw,}$, of the noble gas samples range from 6.85 to 26.18 g, which correspond to wet water contents wc_{wet} of 2.3 – 6.5 wt.% based on the samples' wet weights of 290 – 430 g (Table 2). In the lithologically heterogeneous Passwang Formation, water contents show a large, lithology-related scatter by a factor of more than 2. In the Opalinus Clay, more homogeneous water contents from 3.39 to 6.12 wt.% were measured in the sandy and shaly facies, with one markedly lower value of 2.46 wt.% in the carbonate-rich sandy facies. In the Staffelegg Formation, a water content of 5.92 wt.% was measured. Across all lithologies the water content is positively correlated with the clay content (Waber and Rufer, 2017).

The grain density, ρ_g, was measured on material directly adjacent to the noble gas core samples for the entire Opalinus Clay and Staffelegg Formation. Obtained values scatter

narrowly between 2.69 and 2.71 g/cm^3 with the exception of one higher value of 2.77 g/cm^3 in the carbonate-rich sandy facies of the Opalinus Clay and one significantly lower value of 2.42 g/cm^3 in the bituminous marl of the Staffelegg Formation (Table 2). Due to the lithological heterogeneity of the Passwang Formation, it was not possible to take representative sample material for petrophysical measurements directly adjacent to the noble gas core samples, except for one sample (BDB1-90.86-NG). In consequence, the grain density for rocks of this formation is given as the average value of all samples across the formation (Table 2).

The water loss porosity relative to the wet weight, ϕ_{WLwet}, displays a similar variability and lithological dependency as the water content throughout the profile. The values range from 5.96 to 14.53 vol.% in the Passwang Formation, 6.52 to 15.01 vol.% in the Opalinus Clay and 13.45 vol.% in the Staffelegg Formation (Table 2, Fig. 3).

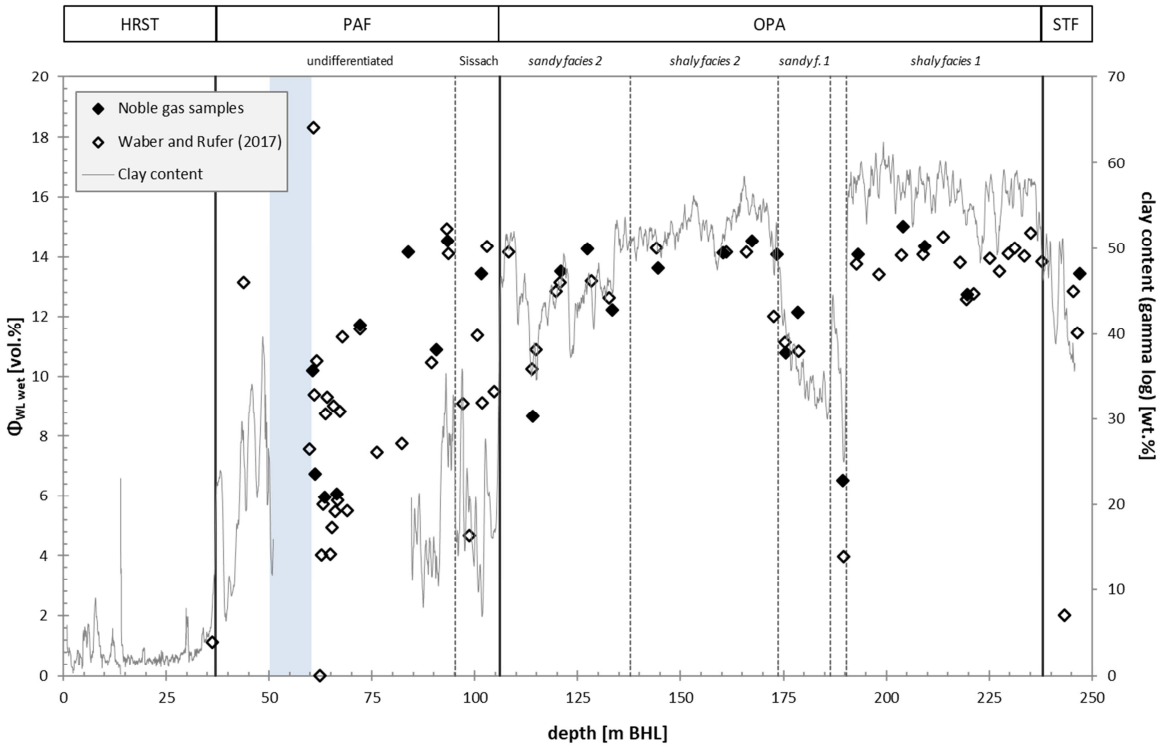

Fig. 3. Water-loss porosity, $\phi_{WL\ wet}$, of the noble gas samples and clay content estimated from the gamma log as a function of depth in borehole BDB-1. The porosity of additional samples measured from BDB-1 (Dataset "Waber and Rufer, 2017") are given for comparison. The packed off interval with the groundwater inflow is shaded in blue. Uncertainties within symbols.

4.2 Porewater and groundwater helium data

Porewater in the Opalinus Clay has $^4He_{pw}$ concentrations between 4.19×10^{-5} and 6.68×10^{-5} ccSTP/g_{pw} in the shaly and sandy facies and one higher value of 9.19×10^{-5} ccSTP/g_{pw} in the carbonate-rich sandy facies. The sample from the Staffelegg Formation shows a $^4He_{pw}$ concentration similar to Opalinus Clay and over both formations a flat profile is established (Fig. 4, Table 3). These $^4He_{pw}$ concentrations are up to 3 orders of magnitude higher than air-saturated water (He_{asw} = 4.6×10^{-8} ccSTP/g_{H2O}; Kipfer et al. 2002), indicating the accumulation of radiogenic ^4He produced in the underground. In contrast $^4He_{pw}$ concentrations continuously decrease from the Opalinus Clay – Passwang Formation interface to values below 1×10^{-6} ccSTP/g_{pw} near the groundwater-conducting feature at 58.6 m BHL. This decrease is about one order of magnitude over the first 30 m into the Passwang Formation to values around 5×10^{-6} ccSTP/g_{pw} measured in the samples at 66.40 and 72.05 m BHL, which seem to form a local plateau. Further up, $^4He_{pw}$ concentrations decrease again sharply by another order of magnitude to the lowest value of 3.09×10^{-7} ccSTP/g_{pw}. This is close to the ^4He concentration of 9.6×10^{-7} ccSTP/g_{gw} of the flowing groundwater at 58.6 m (Waber and Rufer, 2017). While it can be argued that perceiving these second order variations around 70 m BHL could be related to aspects such as a somewhat lower frequency of samples in this interval, the data differ outside the cumulative uncertainties (2.2 - 8.9% 1 RSD; Table 2) and are therefore considered

significant. In addition, the observation of local minima in Cl^- and Br^- concentrations and δ^2H (see discussion below, Fig. 8) and $\delta^{18}O$ signatures in the porewater at the same depth interval (Waber and Rufer, 2017), supports that the observed excursions are the result of changing hydrogeological conditions over time. Porewater $^3He/^4He$ isotope ratios of rock samples from borehole BDB-1 range from 1.42×10^{-7} to 5.85×10^{-7} throughout the Opalinus Clay and the topmost Passwang Formation, with one higher value of 9.12×10^{-7} in the carbonate-rich sandy facies (Fig. 5, Table 3). The data scatter within a narrow range around the $^3He/^4He$ value of 2.39×10^{-7} determined on the groundwater (Waber and Rufer, 2017), with the possible exception of the highest ratio obtained for the carbonate-rich sandy facies.

The porewater $^4He_{pw}$ concentration compare to those obtained by Rübel et al. (2002) from core sections of various boreholes in the Opalinus Clay along the Mont Terri tunnel gallery (2.8×10^{-5} to 9.8×10^{-5} ccSTP/g_{pw}, with a highest value of 1.3×10^{-4} ccSTP/g_{pw} in the carbonate-rich sandy facies). They are also comparable to the $^4He_{pw}$ concentration values of $3.3\text{-}4.8\times10^{-5}$ ccSTP/g_{pw} measured by Maineult et al. (2013) from the sandy facies 1 at the URL level and to the ^4He concentration of 5.14×10^{-4} ccSTP/g determined on water obtained from a wet spot in the Opalinus Clay (Nagra, unpublished data). The $^3He/^4He$ value of 1.54×10^{-7} of this wet spot water is also within the range of the present data.

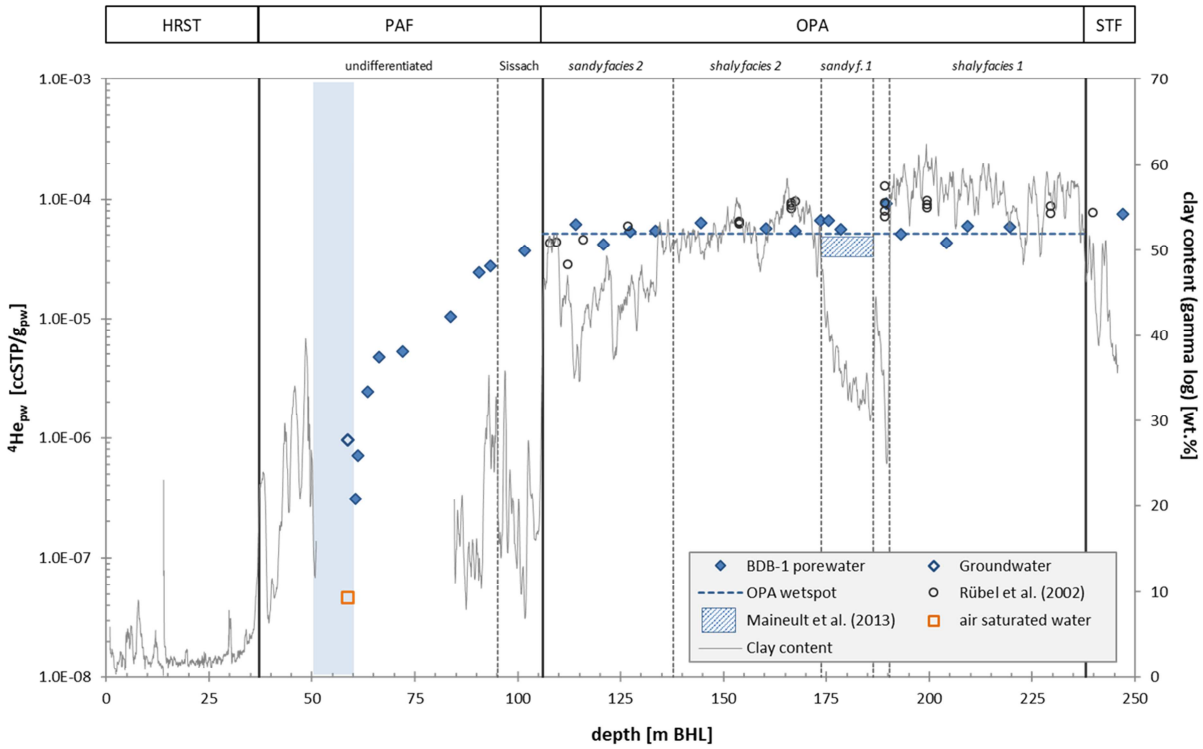

Fig. 4. Concentration of ^{4}He in porewater and groundwater across the Passwang Formation, Opalinus Clay and Staffelegg Formation in borehole BDB-1 at the Mont Terri URL. The packed off interval with the groundwater inflow is shaded in blue. Uncertainties for "BDB-1 porewater" and "groundwater" within symbols.

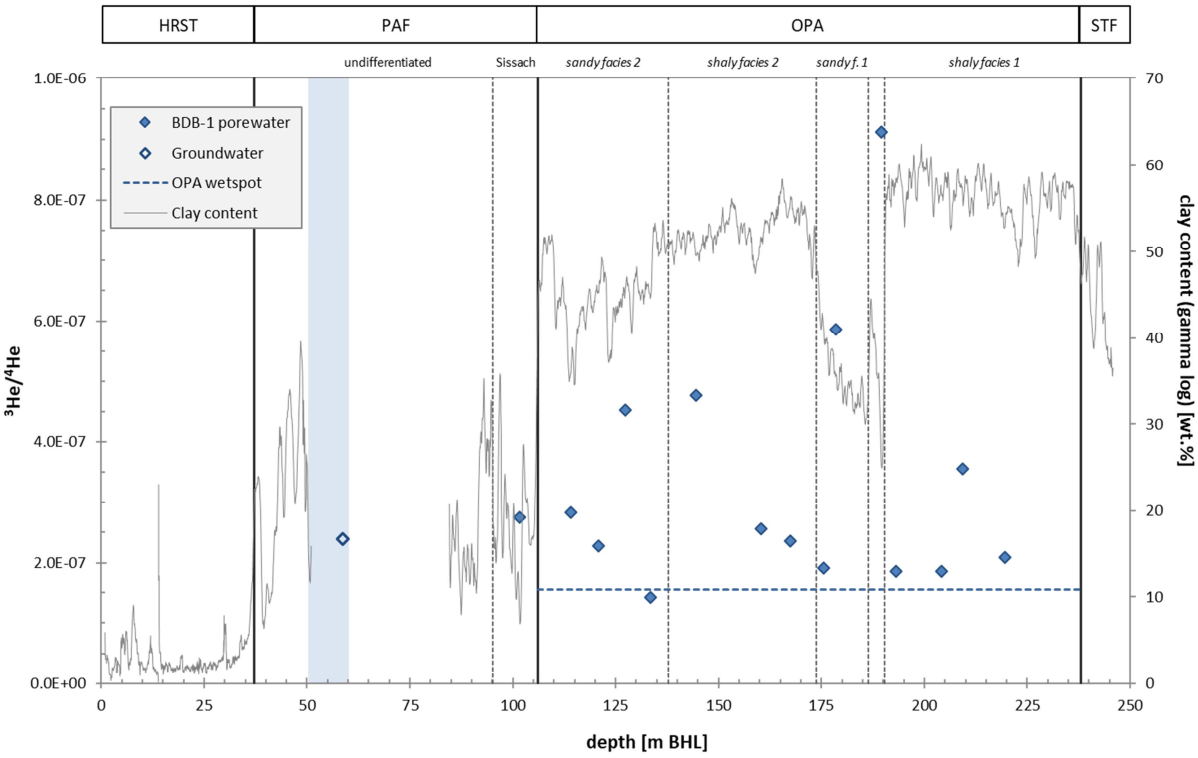

Fig. 5. Ratio of $^3He/^4He$ in porewater and groundwater across the Passwang Formation, Opalinus Clay and Staffelegg Formation in borehole BDB-1 at the Mont Terri URL. The packed off interval with the groundwater inflow is shaded in blue. Uncertainties for "BDB-1 porewater" and "groundwater" within symbols.

Sample	Depth	Formation	Member / Facies	Lithology	ρ_g	$m_{rock\ wet}$	m_{pw}	WC_{wet}	$\phi_{WL\ wet}$
	m BHL				g/cm^3	g	g	wt.%	vol.%
estimated uncertainty (1 SD)					< 0.003	< 0.05	< 0.06	< 0.02	< 0.05
BDB1-60.59-NG	60.59	PAF	undifferentiated	sa lst	*2.76*	321.36	12.98	4.04	10.21
BDB1-61.23-NG	61.23	PAF	undifferentiated	sa lst	*2.76*	337.18	8.79	2.61	6.74
BDB1-63.53-NG	63.53	PAF	undifferentiated.	sa lst	*2.76*	395.82	9.08	2.29	5.96
BDB1-66.40-NG	66.40	PAF	undifferentiated	sa lst	*2.76*	293.30	6.85	2.34	6.07
BDB1-72.05-NG	72.05	PAF	undifferentiated.	sa lst	*2.76*	328.98	15.42	4.69	11.72
BDB1-83.78-NG	83.78	PAF	undifferentiated	mst	*2.76*	340.07	19.58	5.76	14.16
BDB1-90.68-NG	90.68	PAF	undifferentiated.	li sst	2.71	390.12	16.84	4.32	10.89
BDB1-93.40-NG	93.40	PAF	undifferentiated.	sa ma	*2.72*	377.00	22.33	5.92	14.53
BDB1-101.63-NG	101.63	PAF	Sissach-Mb.	sa ma	*2.76*	428.52	23.32	5.44	13.45
BDB1-114.08-NG	114.08	OPA	sandy facies 2	clst & lst la	2.70	355.27	12.06	3.39	8.66
BDB1-120.86-NG	120.86	OPA	sandy facies 2	clst & lst la	2.70	375.89	20.56	5.47	13.51
BDB1-127.33-NG	127.33	OPA	sandy facies 2	clst & lst la	2.70	353.46	20.52	5.80	14.28
BDB1-133.46-NG	133.46	OPA	sandy facies 2	clst & lst la	2.70	317.75	15.59	4.91	12.22
BDB1-144.49-NG	144.49	OPA	shaly facies 2	silt clst	2.70	341.22	18.85	5.52	13.63

BDB1-160.25-NG	160.25	OPA	shaly facies 2	silt clst	2.69	317.00	18.27	5.76	14.14
BDB1-167.38-NG	167.38	OPA	shaly facies 2	silt clst	2.69	374.92	22.26	5.94	14.53
BDB1-173.47-NG	173.47	OPA	shaly facies 2	silt clst	2.70	337.37	19.30	5.72	14.08
BDB1-175.53-NG	175.53	OPA	sandy facies 1	clst & sst la	2.72	388.11	16.51	4.25	10.79
BDB1-178.53-NG	178.53	OPA	sandy facies 1	clst & sst la	2.71	411.46	19.95	4.85	12.15
BDB1-1897.52-NG	189.52	OPA	carb.-rich sandy f.	lst	2.77	434.86	10.70	2.46	6.52
BDB1-193.13-NG	193.13	OPA	shaly facies 1	clst	2.70	407.65	23.36	5.73	14.08
BDB1-204.09-NG	204.09	OPA	shaly facies 1	clst	2.71	427.60	26.18	6.12	15.01
BDB1-209.37-NG	209.37	OPA	shaly facies 1	clst	2.70	351.33	20.54	5.85	14.35
BDB1-219.66-NG	219.66	OPA	shaly facies 1	clst	2.70	416.38	21.36	5.13	12.74
BDB1-246.99-NG	246.99	STF	Rietheim-Mb.	bit ma	2.42	310.92	18.40	5.92	13.45

Grain density values in italics are average values of the entire formation. PAF = Passwang Formation, OPA = Opalinus Clay, STF = Staffelegg Formation. Field lithology after Hostettler et al. (2017): sa lst = sandy limestone, li sst = limy sandstone, sa ma = sandy marl, mst = marlstone, lst = limestone, clst = claystone, silt clst = silty claystone, clst & lst la = claystone with limestone layers, clst & sst la = claystone with sandstone layers, arg ma = argillaceous marl, bit ma = bituminous marl.

Table 2: Petrophysical data of noble gas samples from borehole BDB-1.

Sample	Depth	Formation	Member / Facies	Lithology	$^{4}He_{pw}$	$^{3}He_{pw}/^{4}He_{pw}$	Ne_{pw}
	m BHL				ccSTP/g_{pw}		ccSTP/g_{pw}
estimated uncertainty (1 RSD)					± 2.2 - 8.9% (PAF, STF) ± 1.7 - 2.1% (OPA)	± 0.3 - 2%	± < 3%
BDB1-60.59-NG	60.59	PAF	undifferentiated.	sa lst	3.09E-07		< 1.9E-7
BDB1-61.23-NG	61.23	PAF	undifferentiated.	sa lst	7.09E-07		< 1.9E-7
BDB1-63.53-NG	63.53	PAF	undifferentiated	sa lst	2.43E-06		< 1.9E-7
BDB1-66.40-NG	66.40	PAF	undifferentiated	sa lst	4.72E-06		< 1.9E-7
BDB1-72.05-NG	72.05	PAF	undifferentiated	sa lst	5.29E-06		< 1.9E-7
BDB1-83.78-NG	83.78	PAF	undifferentiated	mst	1.05E-05		< 1.9E-7
BDB1-90.68-NG	90.68	PAF	undifferentiated.	li sst	2.44E-05		< 1.9E-7
BDB1-93.40-NG	93.40	PAF	undifferentiated	sa ma	2.74E-05		9.1E-7
BDB1-101.63-NG	101.63	PAF	Sissach-Mb.	sa ma	3.67E-05	2.75E-07	< 1.9E-7
BDB1-114.08-NG	114.08	OPA	sandy facies 2	clst & lst la	6.11E-05	2.83E-07	1.7E-6
BDB1-120.86-NG	120.86	OPA	sandy facies 2	clst & lst la	4.19E-05	2.28E-07	< 1.9E-7
BDB1-127.33-NG	127.33	OPA	sandy facies 2	clst & lst la	5.39E-05	4.53E-07	1.0E-6
BDB1-133.46-NG	133.46	OPA	sandy facies 2	clst & lst la	5.41E-05	1.42E-07	1.1E-6
BDB1-144.49-NG	144.49	OPA	shaly facies 2	silt clst	6.37E-05	4.78E-07	1.1E-6
BDB1-160.25-NG	160.25	OPA	shaly facies 2	silt clst	5.67E-05	2.56E-07	1.1E-6
BDB1-167.38-NG	167.38	OPA	shaly facies 2	silt clst	5.40E-05	2.36E-07	8.2E-7
BDB1-173.47-NG	173.47	OPA	shaly facies 2	silt clst	6.64E-05		9.6E-7
BDB1-175.53-NG	175.53	OPA	sandy facies 1	clst & sst la	6.68E-05	1.91E-07	1.2E-6
BDB1-178.53-NG	178.53	OPA	sandy facies 1	clst & sst la	5.62E-05	5.85E-07	9.8E-7
BDB1-189.52-NG	189.52	OPA	carb.-rich sandy f.	lst	9.19E-05	9.12E-07	1.9E-6
BDB1-193.13-NG	193.13	OPA	shaly facies 1	clst	5.10E-05	1.86E-07	8.4E-7
BDB1-204.09-NG	204.09	OPA	shaly facies 1	clst	4.33E-05	1.86E-07	7.4E-7
BDB1-209.37-NG	209.37	OPA	shaly facies 1	clst	5.98E-05	3.55E-07	1.0E-6

BDB1-219.66-NG	219.66	OPA	shaly facies 1	clst	5.84E-05	2.09E-07	8.0E-7
BDB1-246.99-NG	246.99	STF	Rietheim-Mb.	bit ma	7.49E-05		1.2E-6

Table 3: Concentration of ^{4}He and Ne and $^{3}He/^{4}He$ ratio in porewater of rock samples from borehole BDB-1. Ne_{pw} values <1.9E-7 ccSTP/g_{pw} indicate that no correction for air-contamination was made, as the measured Ne_{pw} was below the value for air-saturated water (1.9×10^{-7} ccSTP/g_{pw})

4.3 Bulk rock radionuclide and helium data

In the Opalinus Clay, U bulk rock concentrations range from 2.77 – 3.07 ppm in the shaly and sandy facies, with a lower value of 1.54 in the limestones of the carbonate-rich sandy facies (Table 4). Thorium shows a similar concentration pattern in the Opalinus Clay with values between 13.0 and 15.4 ppm and again a lower value of 7.2 ppm in the limestones. The formation's average values weighted by facies thickness calculate to 2.9 ppm U and 14.0 ppm Th, which is similar to the (non-weighted) average values of 2.7 ppm U and 13 ppm Th reported by Lehmann and Tolstikhin (1999) and Rübel et al. (2002) for Opalinus Clay rocks from Mont Terri. The bituminous marl sample from the Staffelegg Formation has a higher U concentration of 4.38 ppm, coupled with a low Th concentration of 6.64 ppm. In the heterogeneous Passwang Formation the only two samples available show a dependence on lithology for U whereas the Th concentrations are similar (Table 4).

Concentrations of ^{4}He in the bulk rock, $^{4}He_{rock}$, range from 4.29×10^{-6} to 1.28×10^{-5} ccSTP/g_{rock} in the Opalinus Clay (Table 4) and compare with the range of $2.5 - 9.8\times10^{-6}$ ccSTP/g_{rock} reported by Lehmann and Tolstikhin (1999).

Fm.	Member / Facies	Thickness	Sample	Lithology	U	Th	$^{4}He_{rock}$	$^{4}He_{prod}$	λ	$^{4}He_{acc}$
		m BHL			ppm	ppm	ccSTP/g_{rock}	ccSTP/(g_{rock}*a)	%	ccSTP/(g_{pw}*a)
estimated uncertainty (1 RSD)					± 10%	± 10%	± 10%			
PAF	undifferentiated	19.98								
PAF	undifferentiated	24.70	BDB1-63.53-NG	sa lst	0.58	11.90	1.05E-05	4.17E-13	85%	1.11E-11

PAF	undifferentiated	13.40	BDB1-93.40-NG	sa ma	2.62	12.10	8.38E-06	6.72E-13	93%	1.11E-11
PAF	Sissach-Mb.	11.00								
OPA	sandy facies 2	31.58	BDB1-127.33-NG	clst & lst la	3.07	15.00	4.34E-06	8.12E-13	97%	1.53E-11
OPA	shaly facies 2	35.97	BDB1-160.25-NG	silt clst	2.92	15.40	4.29E-06	8.05E-13	97%	1.28E-11
OPA	sandy facies 1	12.65	BDB1-178.53-NG	clst & sst la	2.77	13.10	9.36E-06	7.20E-13	93%	1.39E-11
OPA	carb.-rich sandy f.	4.05	BDB1-189.52-NG	lst	1.54	7.20	1.12E-05	3.98E-13	84%	1.32E-11
OPA	shaly facies 1	47.68	BDB1-209.37-NG	clst	2.87	13.00	1.28E-05	7.29E-13	90%	1.09E-11
STF	Rietheim-Mb.		BDB1-246.99-NG	bit ma	4.38	6.64	6.22E-06	7.29E-13	95%	1.10E-11

Formation averages (weighted by thickness of stratigraphic member / facies)

PAF	1.30	11.97	9.73E-06	5.07E-13	88%	1.11E-11
OPA	2.88	13.96	8.06E-06	7.58E-13	94%	1.28E-11
STF	4.38	6.64	6.22E-06	7.29E-13	95%	1.10E-11

Table 4: Radionuclide and ^{4}He concentrations of bulk rock ($^4He_{rock}$), ^{4}He production rates ($^4He_{prod}$) and ^{4}He release coefficients (λ) of rock samples from borehole BDB1, and ^{4}He accumulation rates in porewater ($^4He_{acc}$).

4.4 ^{4}He in-situ production rate, release coefficient and porewater accumulation rate

From the radionuclide data, annual ^{4}He production rates ($^4He_{prod}$) can be calculated according to Ballentine and Burnard (2002) as

$$^4He_{prod} = \frac{3.2422\times10^6\,[U]+7.710\times10^5\,[Th]}{6.022\times10^{23}} \times 22711 \quad [ccSTP\ {g_{rock}}^{-1}\ a^{-1}] \qquad (5)$$

where [U] and [Th] are the bulk rock radionuclide concentrations in ppm, 6.022×10^{23} is Avogadro's constant and the factor 22711 is the molar gas volume in ccSTP/mole (Mohr et al., 2016).

Annual ^{4}He production rates scatter between $7\text{-}8\times10^{-13}$ ccSTP/(g_{rock}*a) for the clay-rich samples of the Opalinus Cay and Staffelegg Formation and with lower values around 4×10^{-13} ccSTP/(g_{rock}*a) for limestones of the Passwang Formation and the carbonate-rich sandy facies of the Opalinus Clay (Table 4).

The fraction λ of the in-situ produced ^{4}He that is released from the rock matrix into the porewater is calculated as

$$\lambda = \frac{(\,^4He_{prod} * t_{sed}) - \,^4He_{rock}}{^4He_{prod} * t_{sed}} \quad (6)$$

where t_{sed} is the average sedimentation age of the formation, which is 168 Ma for the Passwang Formation, 176 Ma for the Opalinus Clay and 180 Ma for the Rietheim Member of the Staffelegg Formation (Mazurek et al. 2009).

The released fraction λ of ^{4}He is generally >90% in clay-rich rocks and distinctly lower in the limestone layers of the Passwang Formation and the carbonate-rich facies of the Opalinus Clay. These layers accordingly also show elevated $^4He_{rock}$ concentrations despite their lower ^{4}He production rates (Table 4).

The released ^{4}He then accumulates in the porewater at an annual rate ($^4He_{acc}$) of

$$^4He_{acc} = \,^4He_{prod} * \lambda * \frac{\rho_g}{\rho_{pw}} * \frac{1-\phi_{WL\,wet}}{\phi_{WL\,wet}} \quad \left[ccSTP\ g_{pw}{}^{-1}\ a^{-1}\right] \quad (7)$$

Calculated annual accumulation rates of ^{4}He in porewater range from 1.1 – 1.5×10^{-11} ccSTP/(g_{pw}*a) (Table 4).

5. Discussion

5.1 ^{4}He in-situ production

The average present day $^4He_{pw}$ concentration in the Opalinus Clay porewater constitutes only about 2.5% of the maximum possible accumulated ^{4}He since the time of sedimentation. This indicates an open system, with either continuous and/or episodic loss of ^{4}He from the porewater in the past. The fraction of $^4He_{pw}$ present in the porewater at Mont Terri is lower compared to the Opalinus Clay in NE Switzerland where this fraction amounts to about

10-45% (Rufer and Waber 2015). This most likely reflects the less quiescent geological history at Mont Terri during the folding of the Jura Mountains.

The minimum duration that would be required to accumulate the today observed $^{4}He_{pw}$ inventory from a completely He-free system and exclusively by in-situ production and total release from the rocks (i.e. in a closed rock-porewater system without influx and/or outflux of He) becomes between 3.4 and 7.0 Ma for the different facies and based on the formations average $^{4}He_{pw}$ inventories. For the Opalinus Clay with an average of 4.4 Ma this is lower than the value of 9.1 Ma calculated by Rübel et al. (2002). These authors, however, used for this calculation their maximum $^{4}He_{pw}$ value obtained in the carbonate-rich sandy facies. Also in the present study the highest $^{4}He_{pw}$ value, together with the highest $^{3}He/^{4}He$ ratio, is obtained for the carbonate-rich sandy facies. However, this maximum value is not considered to be representative for calculating the formation scale minimum build up time, as this positive excursion appears to be the result of a short term He signal (see section 5.4).

5.2 Evaluation of steady-state conditions

The ^{4}He concentration in the Passwang Formation groundwater is approximately 20 times higher than that of infiltrating air-saturated water (Table 1) and ^{4}He in the groundwater is thus derived from the subsurface. The stratigraphic situation indicates a karstic aquifer in the Middle Jurassic Limestones roughly parallel to the top of the Opalinus Clay. With the $^{3}He/^{4}He$ signature of the groundwater closely reflecting the range of values measured in the porewater (Fig. 5), this strongly suggests that the presently observed He in the Passwang Formation groundwater is sourced from the underlying aquitard sequences.

Porewater $^{4}He_{pw}$ concentrations from the water-conducting fracture in the Passwang Formation and across the Opalinus Clay depict a diffusion-type profile shape with a minor,

but significant excursion in the lowermost Passwang Formation, with the flowing groundwater constituting a low concentration upper boundary and almost constant $^4He_{pw}$ concentrations throughout the Opalinus Clay (Fig. 4). A lower boundary with flowing groundwater was not encountered in borehole BDB-1. On the URL level the Late Triassic Gryphaea limestones below the Staffelegg Formation showed observable water flow (Gautschi et al., 1993). Projected to the direction of borehole BDB-1, this stratigraphic unit would appear at 340 m BHL, i.e. almost 100 m below the end of the drilled section.

Rübel et al. (2002) used seepage water from the Gryphaea limestones as the lower boundary for their $^4He_{pw}$ profile along the tunnel level. Based on their $^4He_{pw}$ data (overlain in Fig. 4), and the a priori assumption that the $^4He_{pw}$ system would be in steady-state between in-situ production and diffusive loss to the aquifers above and below the Opalinus Clay, these authors deduced a singular pore diffusion coefficient of 3.5×10^{-11} m^2/s across all lithologies by numerical fitting. Mazurek et al. (2009, 2011) and Jacops et al. (2013) dismiss the assumption of steady-state, as the low value of the pore diffusion coefficient of Rübel et al. (2002) is incompatible with experimentally derived pore diffusion coefficients for ^4He in the Opalinus Clay (Jacops et al. 2013, 2016) and values calculated from experimental HTO diffusion coefficients obtained in the laboratory and in-situ (see 3.6).

Based on these studies and the congruence between this study's $^4He_{pw}$ datasets with that of Rübel et al. (2002), it is unlikely that $^4He_{pw}$ concentrations along the BDB-1 borehole would be in steady-state. To verify this, a steady-state profile between the Passwang Formation groundwater and a groundwater in the Gryphaea limestones was calculated using heterogeneous in-situ porewater He accumulation rates and transport parameters (Table 1) and a fixed groundwater ^4He concentration at the value of air-saturated water

(4.6×10^{-8} ccSTP/g_{H2O}) at both boundaries. The upper half of the modelled steady-state profile is incorporated in Fig. 6. It must be noted that the model is insensitive to setting the He concentration in the boundary groundwaters either to air-saturated water (4.6×10^{-8} ccSTP/g_{H2O}) or the present-day value as measured in the upper boundary in the Passwang Formation (9.6×10^{-7} ccSTP/g_{H2O}), as the absolute concentration difference between these two values and the $^4He_{pw}$ concentration in the centre of the aquitard amounts to less than 2%.

At steady-state, the maximum $^4He_{pw}$ concentration in the Opalinus Clay would be about 6.7×10^{-6} ccSTP/g_{pw} for the given parameters, which is almost an order of magnitude lower than the measured values. For the present-day porewater He concentrations to reach steady-state, a continued and undisturbed evolution under the present day hydrogeological conditions over another 2-5 Ma would be required. This indicates that the present-day porewater He system at Mont Terri is not at steady-state with respect to the observed in-situ He accumulation, transport and boundary parameters, but rather in a transient state from previous situation with more elevated $^4He_{pw}$ concentrations in the Opalinus Clay.

5.3 Porewater evolution model of the Passwang Formation – Opalinus Clay interface

The observed $^4He_{pw}$ concentration profile, with the plateau around 70 m BHL, deviates from a simplistic diffusion profile based on a single upper boundary (i.e. the present day groundwater) and a singular diffusion coefficient over the Passwang Formation. Much more, it suggests a more complex diffusive transport system and history for this upper part of the sediment stack.

In the following, two model scenarios are evaluated: a scenario using a single boundary at constant location and a scenario using a spatially and temporally variable boundary.

The first scenario takes into account the Passwang Formation's lithostratigraphic heterogeneity and the lack of lithology specific diffusion parameters and attributes the observed profile curve to zones of different diffusivity based on lithological differences above and below 76 m BHL (see section 3.6). Modelling the porewater helium profile using the transport and in-situ production parameters given in Table 1 and assuming the present day groundwater flow as singular boundary, results in a relatively good first order fit of the measured concentrations for an activation of the groundwater flow in the Passwang Formation at 58.6 m BHL about 33 ka ago (Fig. 6). Shorter evolution times would overestimate the observed $^{4}He_{pw}$ concentrations in the Passwang Formation whereas longer evolution times would underestimate these across large parts or the entire profile as shown in Figure 6 for evolution times of 1 ka, 100 ka and 1.2 Ma, respectively.

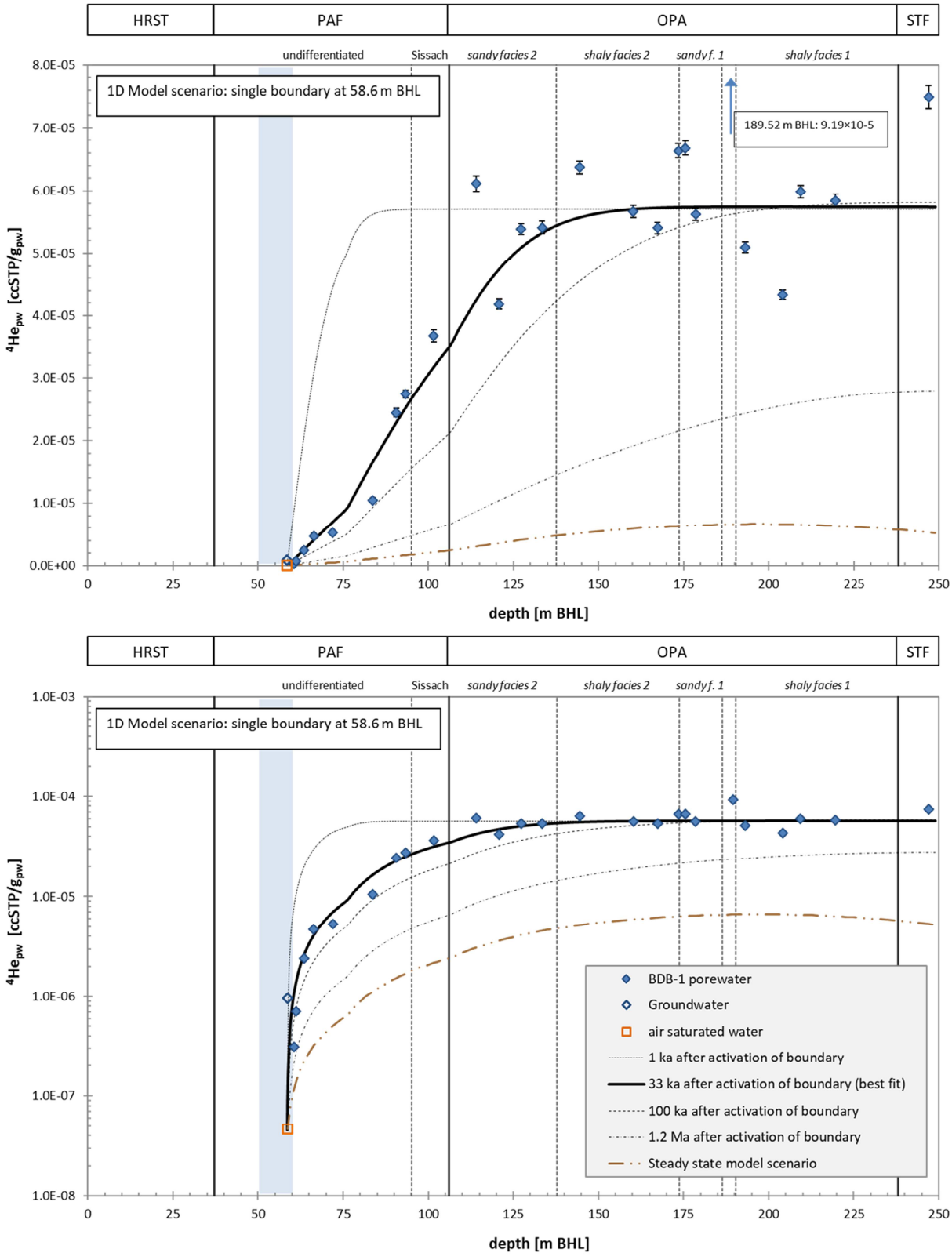

Fig. 6. Model fits of the $^4He_{pw}$ concentration profile across the aquitard sequence towards the groundwater located at 58.6 m BHL as a single boundary (top: linear scale, bottom: logarithmic scale). The model calculation is based on in-situ production,

transport and groundwater parameters given in Table 1. The best fit is obtained for an assumed activation of the aquifer 33 ka ago, while hypothetical activation times of 1 ka, 100 ka and 1.2 Ma clearly over- and underestimate the expected $^4He_{pw}$ concentration profile. The steady-state profile was calculated using the groundwater in the Passwang Formation and assumed flowing groundwater in Triassic limestones at 340 m BHL as boundaries (only the upper half of the profile is shown). The packed off interval with the groundwater inflow is shaded in blue. Uncertainties in the log-scale plot within symbols.

In the second model scenario the drawdown of the $^4He_{pw}$ concentrations by a low ^4He groundwater is assessed by an intermittently active boundary at 73 m BHL which shifts to 58.6 m BHL at a certain time. The existence of this first boundary is based on the excursion in the $^4He_{pw}$ profile and observed open fractures in the drillcore at 72-74 m BHL even though no groundwater flow is detectable in this zone any more.

improved best first order fit between the model curve and the measured porewater helium concentration was obtained when - at first - only the proximal boundary at 73 m BHL was flushed with groundwater with a fixed, air-saturated ^4He concentration from 23 ka to 8 ka ago, with no groundwater flow at 58.6 m BHL during that time. After this period, groundwater flow has ceased at 73 m BHL and has shifted to the present-day location at 58.6 m BHL for the period of 8 ka to present (Fig. 7). During these last 8 ka, the ^4He concentration at the now stagnant boundary at 73 m BHL was no longer fixed and could adjust according to local concentration gradients. Similarly good fits were obtained when the overall model duration and the timing of the boundary change from 73 to 58.6 m BHL were slightly varied, such as flushing from 25-5 ka at 73 m BHL and from 5 ka to present at 58.6 m BHL. For all these simulations, the total evolution time for the present day profile is

between 23 ka and 25 ka and the change in boundary location happens between 5 and 13 ka before present.

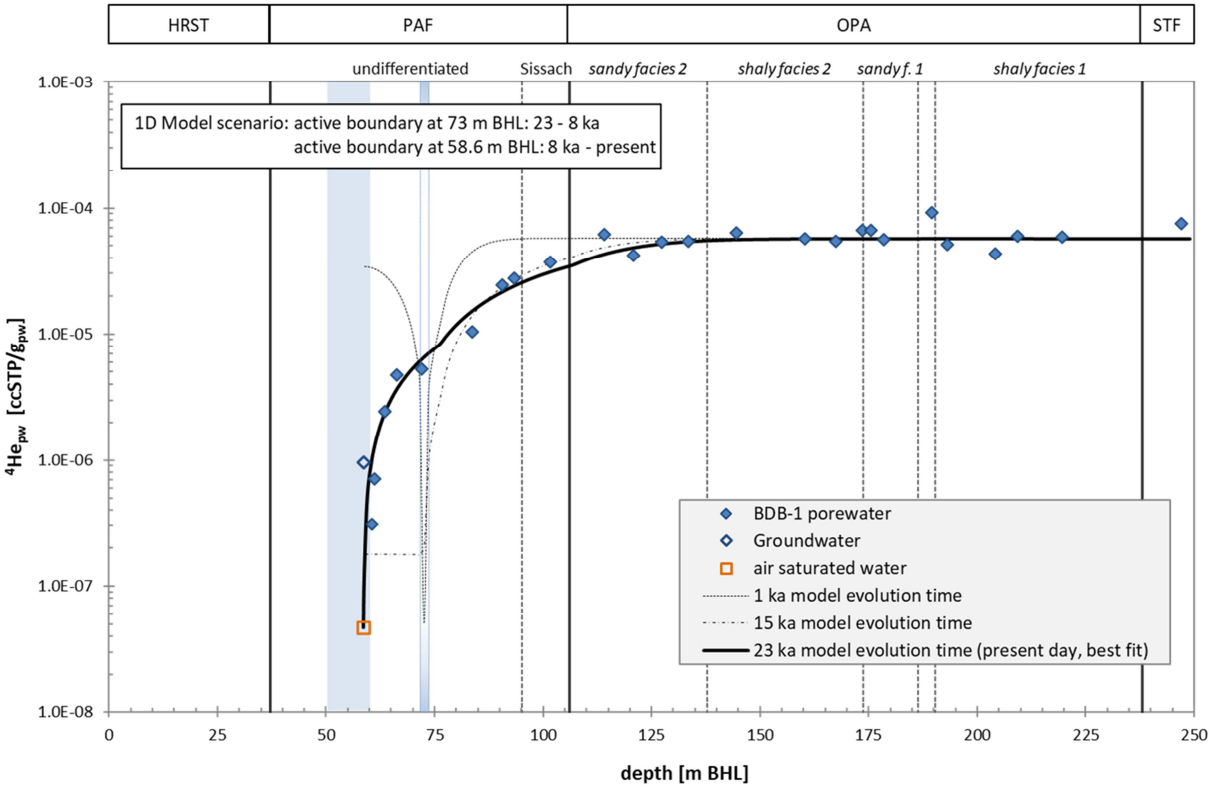

Fig. 7. Model fits of the $^4He_{pw}$ concentration profile across the aquitard sequence towards a spatially variable groundwater boundary. The best fit to the measured data is obtained when the groundwater flow is localised at 73 m BHL from 23 – 8 ka and then shifts to the present day location at 58.6 m BHL, allowing diffusion to continue in this new spatial arrangement for another 8 ka. After the initial activation of groundwater flow only at 73 m BHL, a spatially limited drawdown rapidly establishes on a millennial timescale. Differing in-situ production and diffusive transport parameters (Table 1) above and below the continuing groundwater circulation at 73 m BHL then lead to a skewed $^4He_{pw}$ concentration profile with concentrations between 73 m BHL and 58.6 m BHL well below present day values (illustrated by the 15 ka model evolution time, which is just when the groundwater flow shifts from 73 to 58.6 m BHL). The packed off interval with the groundwater inflow is shaded in

blue and the initial model boundary at 73 m BHL is indicated by the blue gradient rectangle. Uncertainties within symbols.

As can be seen from Fig. 6 and Fig. 7, the resultant model curves for both modelling scenarios are nearly identical. Thus, the existence or influence of such spatial change in the boundary condition is not unequivocally constrained when based solely on helium as a tracer. However, local minima in porewater around 73 m BHL, i.e. the depth of the postulated proximal boundary, are also observed for Cl^- and Br^- concentrations and for δ^2H (Fig. 8) and $\delta^{18}O$ values (Waber and Rufer 2017). Whereas the interpretation of chemical tracer values may be affected by uncertainties associated with the anion-accessible porosity, this is not the case for the stable isotope composition of the water molecule of the porewater. Differences may exist in the development and longevity of these chemical and stable isotope tracer profiles. For the latter, a once established profile may become superimposed by a change in the corresponding signal in the groundwater due to climatic changes during infiltration (e.g. glacial periods) and it may, therefore, not be unambiguously indicative for a spatial dislocation of the boundary. In contrast, for a chemical tracer profile a similar modification due to changes in the chemical composition of the groundwater would require a fundamental change in the hydrogeological system, such as a shift from marine to freshwater infiltration. At Mont Terri, such drastic changes in infiltration conditions for chemical tracers did not occur over the timescale considered here, i.e. since the persisting direct infiltration of freshwater into the Passwang Formation rocks some 1.2 to 2.5 Ma ago. The combined multi-tracer evidence and the observed fractures, however, strongly indicate that groundwater of different composition than the porewater percolated in this zone at 73 m BHL over a certain period.

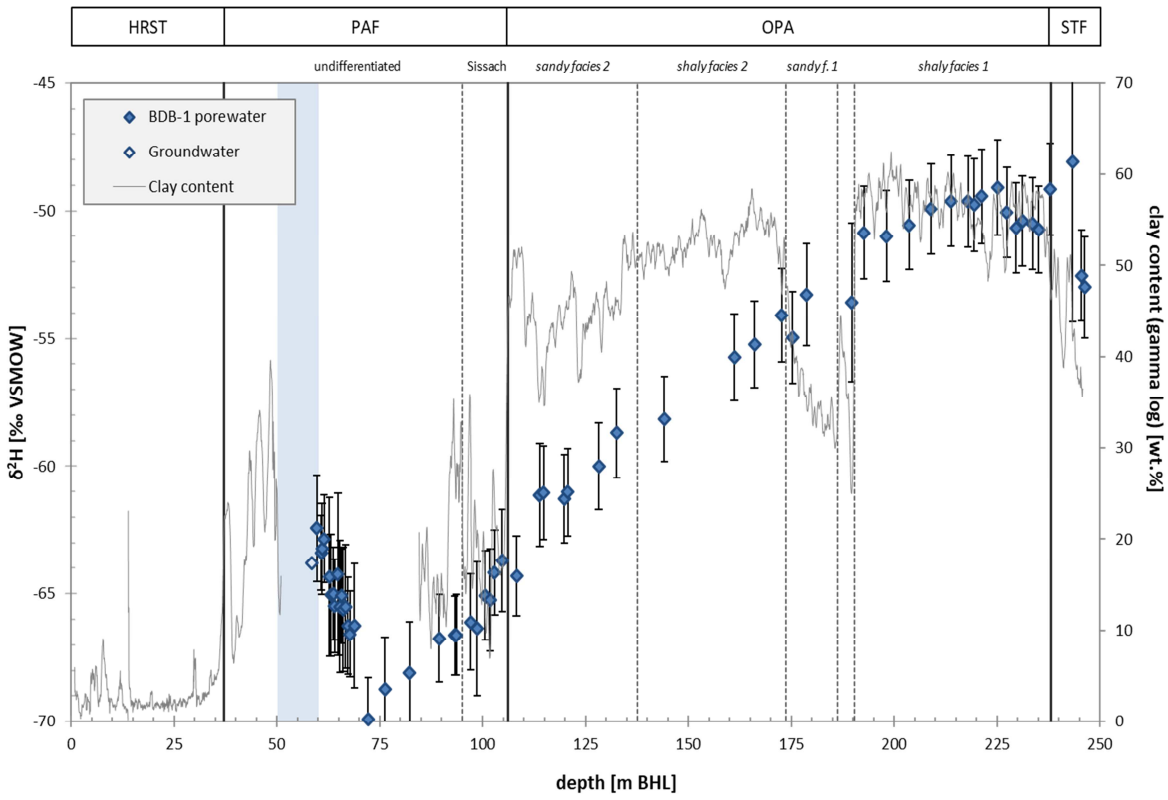

Fig. 8. Values of δ^2H in porewater and groundwater across the Passwang Formation, Opalinus Clay and Staffelegg Formation in borehole BDB-1 at the Mont Terri URL (adapted from Waber and Rufer 2017). The packed off interval with the groundwater inflow is shaded in blue.

Both models presented here do, however, neglect the fact that ^4He concentrations in the groundwater are higher than the air-saturated water concentration assumed in the models.

This higher ^4He groundwater concentration suggests that the model assumption of a perfectly flushed boundary at 58.6 m BHL is not entirely accurate. Based on a steep concentration gradient towards the groundwater such as observed today, a groundwater residence time of less than 500 years would be required to accumulate the measured ^4He concentration in the groundwater. This contrasts the low ^{14}C activity (1.1 ± 0.1 pmC) in the groundwater, which indicates a residence time of 25-29 ka based on chemical and isotope

mass transfer of carbon (Waber and Rufer 2017). If the groundwater at 58.6 m BHL would have been stagnant over such a period of time, the concentration of the accumulated ^{4}He in the groundwater would be a function of the established $^{4}He_{pw}$ concentration gradients.

In the first model scenario the ^{4}He flux across the Passwang Formation into the groundwater at 58.6 m BHL is constrained primarily by the high $^{4}He_{pw}$ concentration in the Opalinus Clay and the heterogeneous diffusivity in the Passwang Formation. Integration of this ^{4}He flux over the groundwater residence time indicated by ^{14}C would yield a hypothetical groundwater ^{4}He concentration of over 2.2×10^{-5} ccSTP/g_{H2O} within 25-29 ka. This is a more than 22 times higher than the measured ^{4}He concentration in the groundwater (9.6×10^{-7} ccSTP/g_{H2O}; Fig. 9).In turn, in the second model scenario, the diffusion path of ^{4}He from the Opalinus Clay to the water conducting zone at 58.6 m BHL is interrupted by the intermittently active water conducting zone at 73 m BHL. This results in low ^{4}He concentrations between 73 and 58.6 m BHL and therefore very low ^{4}He flux into the groundwater over most of the time considered (Fig. 7). As the activation of the 58.6 m BHL boundary in the second model scenario is significantly shorter than the groundwater residence time indicated by ^{14}C, the integration of this lowered flux would result in lower ^{4}He concentrations in the groundwater. For the best-fit solution (23 ka total evolution time, boundary change at 8 ka before present) a ^{4}He concentration in the groundwater of 1.0×10^{-5} ccSTP/g_{H2O} would be reached. For the similarly well-fitting solution with a total evolution time of 25 ka and the boundary change at 5 ka before present, an even lower concentration of 7.0×10^{-6} ccSTP/g_{H2O} is calculated, which is roughly within a factor of 7 of the groundwater value. Despite the predictive value of these calculations being limited by factors such as e.g. the unknown prehistory of the groundwater, it is shown that the second model scenario potentially allows reconciling the $^{4}He_{pw}$ profile and low ^{4}He concentrations

in the groundwater with extended groundwater residence times such as indicated by the ^{14}C activity.

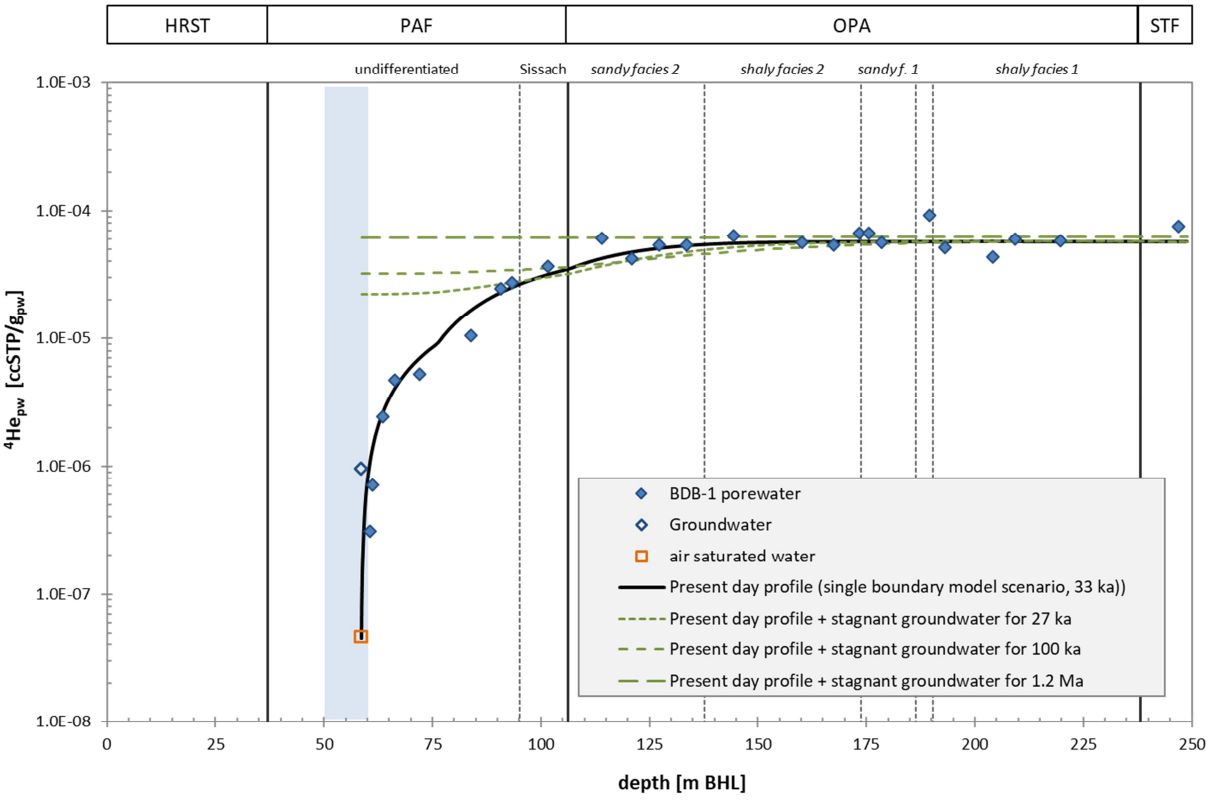

Fig. 9. Modelled $^4He_{pw}$ concentration profiles developing from the present-day profile under closed boundary conditions for variable periods of time. Shown are the resulting modelled 'future' profile shapes if He were accumulating in the groundwater over time periods of 27 ka (average groundwater residence time indicated by ^{14}C), 100 ka, and 1.2 Ma. The present-day profile shape is taken from Fig. 6 and the packed off interval with the groundwater inflow is shaded in blue. Uncertainties within symbols.

5.4 Elevated He signals in the carbonate-rich sandy facies

The highest $^4He_{pw}$ concentration and the highest $^3He/^4He$ ratio were measured in the carbonate-rich sandy facies, with both values being higher by roughly a factor of two

compared to the Opalinus Clay average and the nearest samples outside the carbonate-rich sandy facies. Similarly, Rübel et al. (2002) also report the highest $^4He_{pw}$ concentration in this facies and these authors calculate a minimum build-up time of 9.1 Ma based on this maximum value, compared to the 4.4 Ma based on the average $^4He_{pw}$ concentration in the Opalinus Clay as used here.

High values for both the $^4He_{pw}$ concentration as well as the $^3He/^4He$ ratio cannot be explained by experimental artefacts such as the underestimation of porewater mass. This, together with the agreement between the data by Rübel et al. (2002) and this study, indicates that this excursion represents a hydrogeological signal.

As the excursion in $^4He_{pw}$ values is restricted to the merely 4 m thick limestones, it cannot be explained by any long-term process such as higher (and isotopically lighter) in-situ production. As the diffusion of ^4He is faster than its in-situ production such distinct signal would be transmitted rather quickly from the carbonate-rich sandy facies to the porewater of the surrounding rock. The sample spacing, however, is too large to allow elucidating the processes responsible for this excursion and the time allocated to it. This has to be further elaborated in combination with chemical and water isotope tracers, for which the carbonate-rich sandy facies also appears to have affected the profile shape.

6. Conclusion

Acquisition of ^4He concentration data and $^3He/^4He$ ratios in groundwater, porewater and bulk rock along a spatially finely resolved profile allowed deciphering the complex evolution of a hydrogeological system over an aquifer-aquitard interface in the Opalinus Clay at Mont Terri over the past few ten thousands of years. Helium concentrations in porewater show a diffusion profile towards the aquifer groundwater and a flat shape with values about 2

orders of magnitude higher in the aquitard sequence. The measured average $^4He_{pw}$ concentration of 5.7×10^{-5} ccSTP/g_{pw} in the Opalinus Clay constitutes about 2.5% of the total in-situ produced ^4He since sedimentation. The porewater He system is in a transient state from previously more elevated concentrations. Under the current hydrological conditions the system would reach steady-state in about 2-5 Ma.

Modelled $^4He_{pw}$ concentration profiles show in combination with other chemical and isotopic tracers that the observed $^4He_{pw}$ concentration profiles cannot have evolved exclusively from the opening of the present-day aquifer, but is rather the result of a spatially variable boundary in the karstic system. A best fit with the measured $^4He_{pw}$ data was obtained for a flowing groundwater boundary at 73 m BHL between 23 and 8 ka ago (i.e., for 15 ka) and a subsequent shift of groundwater flow to the present location at 58.6 m BHL.

The data shows that ^4He in porewater reacts quickly to changes in boundary conditions and is capable of resolving and temporally constraining such changes on a scale of a few ka to several 100 ka. As such, excursions in the $^4He_{pw}$ signal are rapidly attenuated. They can easily be missed unless sampling is performed at a high spatial frequency. This is highlighted by the spatially limited excursion of the porewater $^3He/^4He$ ratio (and to a lesser degree the ^4He concentration) in the carbonate-rich sandy facies in the lower half of the Opalinus Clay. An unambiguous interpretation of this local feature would require an even higher sample density.

The characteristics of ^4He being chemically inert and implementing a time indicator via its in-situ production makes it a valuable tracer for investigating aquifer-aquitard interface exchange. In combination with other chemical and isotope tracers, it allows to decipher

temporal and spatial variations of boundary conditions over timescales in the order of 1 ka to 100 ka.

Acknowledgments

D. Jaeggi, L. Wymann, M. Häusler, M. Hoffmann and M. Kern (all swisstopo) are gratefully acknowledged for their support during the borehole BDB-1 core sampling campaign. Analytical support by J. Sültenfuss (Univ. Bremen, Germany), I. Tolstikhin and M. Gannnibal (Kola Scientific Centre, Russia) is highly appreciated. We also thank U. Mäder, P. Wersin and P. Alt-Epping (Univ. Bern), D. Traber (Nagra), A. Vinsot (Andra) and M. Suchy for many fruitful discussions and comments over the course of this work. The constructive criticism of A. Bath and two anonymous reviewers helped to further improve the manuscript. The project was carried out within the Mont Terri DB- and DB-A-Experiments, financed by swisstopo, IRSN, Nagra, and NWMO.

References

Ballentine, C.J., Burnard, P.G., 2002. Production, release and transport of noble gases in the continental crust. *In*: Porcelli D., Ballentine, C.J., Wieler, R., Noble Gases in Geochemistry and Cosmochemistry, Reviews in Mineralogy & Geochemistry 47, Min. Soc. of America, Washington D.C., 481-538.

Battani, A., Smith, T., Robinet, J.C., Brulhet, J., Lavielle, B., Coelho, D., 2011. Contribution of logging tools to understanding helium porewater data across the Mesozoic sequence of the East of the Paris Basin. Geochim. Cosmochim. Acta 75, 7566-7584.

Bensenouci, F., Michelot, J.L., Matray, J.M., Savoye, S., Lavielle, B., Thomas, B., Dick, P., 2011. A profile of helium-4 concentration in pore-water for assessing the transport phenomena through an argillaceous formation (Tournemire, France). Phys. Chem. Earth 36, 1521-1530.

Beyerle, U., Aeschbach-Hertig, W., Imboden, D.M., Baur, H., Graf, T., Kipfer, R., 2000. A mass spectrometric system for the analysis of noble gases and tritium from water samples. Environ. Sci. Technol. 34, 2042-2050.

Bigler, T., Ihly, B., Lehmann, B.E., Waber, H.N., 2005. Helium Production and Transport in the Low-Permeability Callovo-Oxfordian Shale at the Site Meuse/Haute Marne, France. Nagra Arbeitsbericht NAB 05-07, Wettingen, Switzerland, *www.nagra.ch*.

Bossart, P., Bernier, F., Birkholzer, J., Bruggeman, C., Connolly, P., Dewonck, S., Fukaya, M., Herfort, M., Jensen, M., Matray, J.M., Mayor, J.C., Moeri, A., Oyama, T., Schuster, K., Shigeta, N., Vietor, T., Wieczorek, K., 2017. Mont Terri rock laboratory, 20 years of research: introduction, site characteristics and overview of experiments. Swiss J. Geosci. 110, 3-22.

Bossart, P., Wermeille, S., 2003. Paleohydrological study of the Mont Terri rock laboratory., in: Heitzmann, P., Tripet, J.P. (Eds.), Mont Terri Project – Geology, paleohydrogeology and stress field of the Mont Terri region. Federal Office for Water and Geology Rep. 4, Bern, Switzerland, 45–64, *www.swisstopo.admin.ch*.

Clark, I.D., Al, T., Jensen, M., Kennell, L., Mazurek, M., Mohapatra, R., Raven, K.G., 2013. Paleozoic-aged brine and authigenic helium preserved in an Ordovician shale aquiclude. Geology 41, 951-954.

Cook, P.G., Herczeg, A.L., 2000. Environmental tracers in subsurface hydrology. Kluwer Academic Publishers, Boston, Dordrecht, London.

de Laeter, J.R., Böhlke, J.K., de Bièvre, P., Hidaka, H., Peiser, H.S., Rosman, K.J.R., Taylor, P.D.P., 2003. Atomic weights of the elements : Review 2000. Pure App. Chem.75, 683-800.

Falck, W.E., Bath, A.H., Hooker, P.J., 1990. Long-term solute migration profiles in clay sequences. Z. Dtsch. Geol. Ges. 141, 415-426.

Fischer, D., 2014. DB experiment: Borehole Logging Mont Terri Test Site, in the borehole BDB1 18.12.2013, 13.1.2014 and 30.1.2014. Mont Terri Technical Note 2014-29, Federal Office of Topography (swisstopo), Wabern, Switzerland, *www.mont-terri.ch*.

Gautschi, A., Ross, C., Scholtis, A., 1993. Porewater–groundwater relationships in Jurassic shales and limestones of northern Switzerland. *In*: Manning, D.A.C., Hall, P.L., Hughes, C.R. (Eds.), Geochemistry of Clay–Pore Fluid Interactions. Mineral Soc. Serie 4, Chapman & Hall, London, 412–422.

Gimmi, T., Waber, H.N., 2004. Modelling of tracer profiles in pore water of argillaceous rocks in the Benken borehole: stable water isotopes, chloride and chlorine isotopes. Nagra Technical Report NTB 04-05, Wettingen, Switzerland, *www.nagra.ch*.

Gimmi, T., Waber, H.N., Gautschi, A., Rübel, A., 2007. Stable water isotopes in pore water of Jurassic argillaceous rocks as tracers for solute transport over large spatial and temporal scales. Water Resour. Res. 43, W04410, doi:10.1029/2005WR004774.

Gómez-Hernández, J.J., 2000. FM-C Experiment: Part A) Effective Diffusivity and Accessible Porosity Derived from in-situ He-4 Tests. Part B) Prediction of He-3 Concentration in a Cross-Hole Experiment. Mont Terri Project Technical Note 2000-40. Federal Office of Topography (swisstopo), Wabern, Switzerland, *www.mont-terri.ch*.

Hostettler, B., Reisdorf, A.G., Jaeggi, D., Deplazes, G., Blasi, H., Morard, A., Feist-Burkhardt, S., Waltschew, A., Dietze, V., Menkveld-Gfeller, U., 2017. Litho- and biostratigraphy of the Opalinus Clay and bounding formations in the Mont Terri rock laboratory (Switzerland). Swiss J. Geosci. 110, 23-37.

Jacops, E., Volckaert, G., Maes, N., Weetjens, E., Govaerts, J., 2013. Determination of gas diffusion coefficients in saturated porous media: He and CH_4 diffusion in Boom Clay. Appl. Clay Sci. 83-84, 217-223.

Jacops, E., Maes, N., Bruggeman, C., Grade, A., 2016. Measuring diffusion coefficients of dissolved He and Ar in three potential clay host formations Boom Clay, Callovo Oxfordian Clay and Opalinus Clay. *In*: Norris, S., Bruno, J., Van Geet, M., Verhoef, E. (Eds.), Radioactive Waste Confinement: Clays in Natural and Engineered Barriers. Geological Society, London, England.

Jaeggi, D., Kern, N., Hoffmann, M., Wymann, L., 2016. DB (Deep inclined borehole through the Opalinus Clay) Experiment, Borehole BDB-1 (247.5 m), Report of on-site operations, geological core mapping, sampling, installation of multipacker system and first results. Mont Terri Project Technical Note 2015-124. Federal Office of Topography (swisstopo), Wabern, Switzerland, *www.mont-terri.ch*.

Jaeggi, D., Laurich, B., Nussbaum, C., Schuster, K., Connolly, P., 2017. Tectonic structure of the "Main Fault" in the Opalinus Clay, Mont Terri rock laboratory (Switzerland). Swiss J. Geosci. 110, 67-84.

Jean-Baptiste, P., Lavielle, B., Fourré, E., Smith, T., Pagel, M., 2016. Vertical distribution of helium and $^{40}Ar/^{36}Ar$ in porewaters of the Eastern Paris Basin (Bure/Haute Marne): Constraints on transport processes through the sedimentary sequence. Geological Society, London, Special Publications 443.

Kipfer, R., Aeschbach-Hertig, W., Peeters, F., Stute, M., 2002. Noble gases in lakes and ground waters. *In*: Porcelli D., Ballentine, C.J., Wieler, R., Noble Gases in Geochemistry and Cosmochemistry, Reviews in Mineralogy & Geochemistry 47, Min. Soc. of America, Washington D.C., 615-700.

Lehmann, B.E., Tolstikhin, I.N., 1999. Noble gases and isotopes from porewaters and rocks, Part II: Helium and Argon Isotopes in Rock Samples. *In*: Thury, M., Bossart, P. (Eds.), Mont Terri Rock Laboratory – Results of the hydrogeoglogical, geochemical and geotechnical experiments performed (1996-1997), Reports of the Federal Office of Water and Geology (FOWG), Geological Report No 23. Federal Office of Topography (swisstopo), Wabern, Switzerland, p. 148-151, *www.swisstopo.admin.ch*.

Leya, I., Wieler, R., 1999. Nucleogenic production of Ne isotopes in Earth's crust and upper mantle induced by alpha particles from the decay of U and Th. J. Geophys. Res. 104, 15439-15450.

Lichtner, P.C., 2007. FLOTRAN Users Manual: Two-phase Non-Isothermal Coupled Thermal-Hydrologic-Chemical (THC) Reactive Flow and Transport Code Version 2. Los Alamos National Laboratory, New Mexico, U.S.A.

Maineult, A., Thomas, B., Nussbaum, C., Wieczorek, K., Gibert, D., Lavielle, B., Kergosien, B., Nicollin, F., Mahiouz, K., Lesparre, N., 2013. Anomalies of noble gases and self-potential associated with fractures and fluid dynamics in a horizontal borehole, Mont Terri Underground Rock Laboratory. Eng. Geol. 156, 46-57.

Mazurek, M., Hurford, A.J., Leu, W., 2006. Unravelling the multi-stage burial history of the Swiss Molasse Basin: integration of apatite fission track, vitrinite reflectance and biomarker isomerisation analysis. Basin Res. 18, 27-50.

Mazurek, M., Alt-Epping, P., Bath, A., Gimmi, T., Waber, H.N., 2009. Natural tracer profiles across argillaceous formations: The CLAYTRAC Project. OECD/NEA Rep. 6253, OECD Nuclear Energy Agency, Paris, France, *www.oecdbookshop.org*.

Mazurek, M., Alt-Epping, P., Bath, A., Gimmi, T., Waber, H.N., Buschaert, S., De Canniere, P., De Craen, M., Gautschi, A., Savoye, S., Vinsot, A., Wemaere, I., Wouters, L., 2011. Natural tracer profiles across argillaceous formations. App. Geochem. 26, 1035-1064.

Mazurek, M., Al, T., Celejewski, I.D., Clark, I., Fernández, A.M., Jaeggi, D., Kennell-Morrison, L., Matray, J.M., Murseli, S., Oyama, T., Qiu, S., Rufer, D., St-Jean, G., Waber, H.N., Yu, C., 2017. Mont Terri Project: Mont Terri DB-A Experiment: Comparison of Pore-water Investigations Conducted by Several Research Groups on Core Materials from the BDB-1 Borehole. NWMO Technical Report TR-2017-09, Nuclear Waste Management Organization, Toronto Canada, *www.nwmo.ca*.

Mohr, P.J., Newell, D.B., Taylor, B.N., 2016. CODATA Recommended Values of the Fundamental Physical Constants: 2014. J. Phys. Chem. Ref. Data 45.

Nagra, 2001. Sondierbohrung Benken, Untersuchungsbericht. Nagra Technical Report NTB 00-01, Wettingen, Switzerland, *www.nagra.ch*.

Nagra, 2002. Projekt Opalinuston – Synthese der geowissenschaftlichen Untersuchungsergebnisse. Entsorgungsnachweis für abgebrannte Brennelemente, verglaste hochaktive sowie langlebige mittelaktive Abfälle. Nagra Technical Report NTB 02-03, Nagra, Wettingen, Switzerland, *www.nagra.ch*.

Nussbaum, C., Bossart, P., Amann, F., Aubourg, C., 2011. Analysis of tectonic structures and excavation induced fractures in the Opalinus Clay, Mont Terri underground rock laboratory (Switzerland). Swiss J. Geosci. 104, 187-210.

Nussbaum, C., Kloppenburg, A., Caer, T., Bossart, P., 2017. Tectonic evolution around the Mont Terri rock laboratory, northwestern Swiss Jura: constraints from kinematic forward modelling. Swiss J. Geosci. 110, 39-66.

Osenbrück, K., Lippmann, J., Sonntag, C., 1998. Dating very old pore waters in impermeable rocks by noble gas isotopes. Geochim. Cosmochim. Acta 62, 3041-3045.

Palut, J.M., Montarnal, P., Gautschi, A., Tevissen, E., Mouche, E., 2003. Characterisation of HTO diffusion properties by an in situ tracer experiment in Opalinus clay at Mont Terri. J. Contam. Hydrol. 61, 203-218.

Pearson, F.J., Arcos, D., Bath, A., Boisson, J.-Y., Fernández, A.M., Gäbler, H.-E., Gaucher, E., Gautschi, A., Griffault, L., Hernán, P., Waber, H.N., 2003. Mont Terri Project – Geochemistry of Water in the Opalinus Clay Formation at the Mont Terri Rock Laboratory. Reports of the Federal Office of Water and Geology (FOWG), Geology Series No 5. Federal Office of Topography (swisstopo), Wabern, Switzerland, 319pp, *www.swisstopo.admin.ch*.

Poole, J.C., McNeill, G.W., Langman, S.R., Dennis, F., 1997. Analysis of noble gases in water using a quadrupole mass spectrometer in static mode. App. Geochem. 12, 707-714.

Reisdorf, A.G., Hostettler, B., Waltschew, A., Jaeggi, D., Menkveld-Gfeller, U., 2014. SO (Sedimentology of the Opalinus-Ton) Biostratigraphy of the Basal Part of the Opalinus-Ton at the Mont Terri rock laboratory, Switzerland. Mont Terri Technical Report TR 14-07, Federal Office of Topography (swisstopo), Wabern, Switzerland, *www.mont-terri.ch*.

Rübel, A.P., Sonntag, C., Lippmann, J., Pearson, F.J., Gautschi, A., 2002. Solute transport in formations of very low permeability: Profiles of stable isotope and dissolved noble gas contents of pore water in the Opalinus Clay, Mont Terri, Switzerland. Geochim. Cosmochim. Acta 66, 1311-1321.

Rufer, D., Waber, H.N., 2015. Noble and reactive gas data of porewaters and rocks from the Schlattingen borehole SLA-1, Nagra Arbeitsbericht NAB 15-012, Wettingen, Switzerland, *www.nagra.ch*.

Savoye, S., Michelot, J.L., Bensenouci, F., Matray, J.M., Cabrera, J., 2008. Transfers through argillaceous rocks over large space and time scales: Insights given by water stable isotopes. Phys. Chem. Earth 33, S67-S74.

Sültenfuss, J., Roether, W., Rhein, M., 2009. The Bremen mass spectrometric facility for the measurement of helium isotopes, neon, and tritium in water. Isotopes in Environmental and Health Studies 45, 83-95.

Tevissen, E., Soler, J.M., 2003. In Situ Diffusion Experiment (DI): Synthesis Report. Mont Terri Technical Report TR 2001-05, Federal Office of Topography (swisstopo), Wabern, Switzerland, 56pp., *www.mont-terri.ch*.

Tevissen, E., Soler, J.M., Montarnal, P., Gautschi, A., Van Loon, L.R., 2004. Comparison between in situ and laboratory diffusion studies of HTO and halides in Opalinus Clay from the Mont Terri. Radiochim. Acta 92, 781-786.

Tolstikhin I.N., Waber H.N. Kamensky I.L., Loosli H.H., Skiba V.I., Gannibal M.A., 2011. Production, redistribution and loss of helium and argon isotopes in a thick sedimentary aquitard-aquifer system (Molasse Basin, Switzerland). Chem. Geol. 286, 48-58.

Van Loon, L., 2014. Effective Diffusion Coefficients and Porosity Values for Argillaceous Rocks and Bentonite: Measured and Estimated Values for the Provisional Safety Analyses for SGT-E2. Nagra Technical Report NTB 12-03, Wettingen, Switzerland, 130 pp, *www.nagra.ch*.

Van Loon, L.R., Soler, J.M., Muller, W., Bradbury, M.H., 2004a. Anisotropic diffusion in layered argillaceous rocks: A case study with opalinus clay. Environ. Sci. Technol. 38, 5721-5728.

Van Loon, L.R., Wersin, P., Soler, J.M., Eikenberg, J., Gimmi, T., Hernan, P., Dewonck, S., Savoye, S., 2004b. In-situ diffusion of HTO, $^{22}Na^{+}$, Cs^{+} and I^{-} in Opalinus Clay at the Mont Terri underground rock laboratory. Radiochim. Acta 92, 757-763.

Van Loon, L.R., Muller, W., Iijima, K., 2005. Activation energies of the self-diffusion of HTO, $^{22}Na^{+}$ and $^{36}Cl^{-}$ in a highly compacted argillaceous rock (Opalinus Clay). App. Geochem. 20, 961-972.

Waber, H.N., 2012. Laboratoire de Recherche Souterrain Meuse / Haute-Marne - Geochemical Data of Borehole EST433, Nagra Arbeitsbericht NAB 09-16, Wettingen, Switzerland, *www.nagra.ch*.

Waber, H.N., Gimmi, T., Smellie, J.A.T., 2012. Reconstruction of palaeoinfiltration during the Holocene using porewater data (Laxemar, Sweden). Geochim. Cosmochim. Acta 94, 109–127, DOI: 10.1016/j.gca.2012.06.030.

Waber, H.N., Rufer, D., 2017. Porewater Geochemistry, Method Comparison and Opalinus Clay – Passwang Formation Interface Study at the Mont Terri URL. NWMO Technical Report TR-2017-10, Nuclear Waste Management Organization, Toronto Canada, *www.nwmo.ca*.

Weiss, R.F., 1971. Solubility of Helium and Neon in Water and Seawater. J. Chem. Eng. Data 16, 235-241.

Wersin, P., Van Loon, L.R., Soler, J.M., Yllera, A., Eikenberg, J., Gimmi, T., Hernan, P., Boisson, J.Y., 2004. Long-term diffusion experiment at Mont Terri: first results from field and laboratory data. Appl. Clay Sci. 26, 123-135.

Wersin, P., Soler, J.M., Van Loon, L., Eikenberg, J., Baeyens, B., Grolimund, D., Gimmi, T., Dewonck, S., 2008. Diffusion of HTO, Br^{-}, I^{-}, Cs^{+}, $^{85}Sr^{2+}$ and $^{60}Co^{2+}$ in a clay formation: Results and modelling from an in situ experiment in Opalinus Clay. App. Geochem. 23, 678-691.

Willenberg-Spillmann, H., 2015. Bohrung BDB-1 (Mont Terri): Abschätzung des Tonmineralgehaltes aus geophysikalischen Bohrlochlogs. *Appendix in Reisdorf et al. (2016)*, Litho- and biostratigraphy of the 250 m-deep Mont Terri BDB-1 borehole

through the Opalinus Clay and bounding formations. Mont Terri Technical Report TR 2016-02, Federal Office of Topography (swisstopo), Wabern, Switzerland, *www.mont-terri.ch*.

Yu, C., 2017. Comparative study of convective and diffusive transport phenomena within the Opalinus Clay at Mont Terri, École doctorale 251 - Sciences de l'environnement. PhD Thesis, Université d'Aix-Marseille, France.

Yu, C., Matray, J.M., Goncalves, J., Jaeggi, D., Grasle, W., Wieczorek, K., Vogt, T., Sykes, E., 2017. Comparative study of methods to estimate hydraulic parameters in the hydraulically undisturbed Opalinus Clay (Switzerland). Swiss J. Geosci. 110, 85-104.

Rufer, Waber and Gimmi - Identifying temporally and spatially changing boundary conditions at an aquifer – aquitard interface using helium in porewater

Research highlights:

- Porewater He data over an aquifer-aquitard interface at Mont Terri show a transient state diffusion profile.
- Porewater He concentrations range from 0.3-90×10^{-6} ccSTP/g_{pw}, with $^{3}He/^{4}He$ ratios between 1.4-9.1×10^{-7}.
- Combining He porewater evolution models with independent chemical and isotopic tracers allow deciphering a complex palaeo-hydrogeological history over the last 30 ka.